

# Leptogenesis in an extended seesaw model with $U(1)_{B-L}$ symmetry

Ujjal Kumar Dey<sup>a,1</sup> Tapoja Jha<sup>b,2</sup> Ananya Mukherjee<sup>c,3</sup> Nirakar Sahoo<sup>a,d,4</sup>

<sup>a</sup> *Department of Physical Sciences, Indian Institute of Science Education and Research  
Berhampur, Transit Campus, Government ITI, Berhampur 760010, Odisha, India*

<sup>b</sup> *Kolkata, India*

<sup>c</sup> *Theoretical Physics Division, Physical Research Laboratory, Ahmedabad 380009, India*

<sup>d</sup> *Center of Excellence in High Energy and Condensed Matter Physics, Department of  
Physics, Utkal University, Bhubaneswar 751004, India*

## Abstract

We have explored an extended seesaw model accommodating a keV sterile neutrino adopting  $U(1)_{B-L}$  symmetry. This model provides a natural platform for achieving resonant leptogenesis to account for the observed baryon asymmetry of the Universe. The required lepton asymmetry is sourced by the CP violating decay of the lightest heavy right handed neutrino to Standard Model leptons and Higgs. The presence of the light sterile neutrino in the model brings out an enhancement in the final lepton asymmetry through an additional self-energy contribution. Adopting a proper treatment for all the washout processes this framework strictly favours a strong washout regime thereby protecting the low energy neutrino mass parameters in agreement with the present neutrino and cosmology data. This framework of extended seesaw scheme offers the source of matter-antimatter asymmetry without any severe fine tuning of the Yukawa couplings governing the tiny neutrino mass. We also comment on the half-life period for the neutrino less double beta decay process in the background of having a keV sterile neutrino satisfying all the constraints which guide the explanation for the observed baryon asymmetry of the Universe.

---

<sup>1</sup>E-mail: [ujjal@iiserbpr.ac.in](mailto:ujjal@iiserbpr.ac.in)

<sup>2</sup>E-mail: [tapoja.phy@gmail.com](mailto:tapoja.phy@gmail.com)

<sup>3</sup>E-mail: [ananya@prl.res.in](mailto:ananya@prl.res.in)

<sup>4</sup>E-mail: [nirakar.pintu.sahoo@gmail.com](mailto:nirakar.pintu.sahoo@gmail.com)

---

## Contents

<b>1</b>	<b>Introduction</b>	<b>1</b>
<b>2</b>	<b>Model description</b>	<b>3</b>
2.1	Field content and interactions . . . . .	3
2.2	Neutrino Mass generation through extended seesaw mechanism . . . . .	5
2.3	Constraints on model parameters . . . . .	5
<b>3</b>	<b>Numerical analysis of extended seesaw parameter space</b>	<b>6</b>
3.1	ESS paramater space . . . . .	7
<b>4</b>	<b>Baryogenesis through leptogenesis</b>	<b>11</b>
4.1	Lepton asymmetry parameter . . . . .	11
4.2	Boltzmann Equations . . . . .	11
<b>5</b>	<b>Results and analysis</b>	<b>12</b>
5.1	Parameter space for leptogenesis . . . . .	12
<b>6</b>	<b>Neutrinoless double beta decay</b>	<b>15</b>
<b>7</b>	<b>Conclusion</b>	<b>17</b>

---

## 1 Introduction

After the youngest discovery of the Standard Model (SM) predictions in terms of the Higgs boson, it is needless to say that the SM is one of the most successful theories of particle physics dealing with the matter and their fundamental interacting forces. In spite of this huge success, there remain a number of limitations of the SM in the context of explaining the origin of neutrino mass, existence of dark matter (DM) and the reason behind the predominance of matter over antimatter in our observable Universe. In the past decades, there have been plenty of theoretical studies with an objective of addressing the above mentioned issues at the cost of constructing some beyond standard model (BSM) frameworks [1, 2]. In order to account for tiny neutrino mass one of the most economical possibilities is to embed a seesaw mechanism [3–6] into the SM. Over the years a host of seesaw scenarios are proposed. The various seesaw models can also have phenomenological importance in the context of probing them in the colliders. Among the variants of the seesaw schemes low-scale seesaw mechanisms have gained considerable attention in view of their testability in the colliders [7, 8]. Within the same seesaw framework testing leptogenesis is another probe to validate the neutrino mass generation mechanism from the perspective of various cosmological observations.

The matter-antimatter asymmetry can be parametrised by the baryon to photon ratio. Various cosmological observations report this ratio to be [9]

$$\eta_B = \frac{n_B - n_{\bar{B}}}{n_\gamma} = (2.6 - 6.2) \times 10^{-10} \quad (1)$$

where  $n_B$ ,  $n_{\bar{B}}$ ,  $n_\gamma$  and  $s$  represent number densities of baryons, antibaryons, photons, and entropy respectively. A very appealing and field theoretically consistent mechanism of generating the baryon asymmetry of the Universe is the process of leptogenesis which was first

pointed out by Fukugita and Yanagida [10]. Leptogenesis, being a direct consequence of the seesaw models having right handed neutrinos (RHN) also establishes a connection between the origin of neutrino mass and the baryon asymmetry of the Universe. Realization of baryogenesis through leptogenesis via the decay of RHN in various seesaw models can be found in [7, 11–15]. For a recent review one may look at [16, 17] and the references there in. These RHNs can in principle be uncharged under the SM gauge interactions; unless protected by some new symmetry they would mix with the active neutrinos. Inclusion of a pair of sterile neutrinos to the SM fermion sector has become a common lore in order to explain the tiny neutrino mass through type-I seesaw mechanism [16, 18–21]. Type-I seesaw model predicts a bound on the sterile neutrino mass to be very heavy ( $M \sim 10^{14}$  GeV) in order to generate the correct light neutrino masses. However, considering sterile neutrinos at accessible energies gained considerable attention in the last decade from the perspective of being probed directly at high energy collider LHC. Interestingly, the most appealing window for sterile neutrino mass has been seen to be from 1 eV to 10 TeV which also has theoretical and experimental incentives. In the context of realizing a low scale leptogenesis a mechanism called resonant-leptogenesis [22–24] has become popular in the past decade. This can be perceived as follows: due to the presence of two quasi-degenerate RH neutrinos, the CP asymmetry parameter which quantifies the leptogenesis process gets resonantly enhanced and opens up possibilities for successful leptogenesis even at RH mass scale  $\mathcal{O}(\text{TeV})$ .

In this work we utilise a  $U(1)_{B-L}$  extension of the SM based on extended seesaw mechanism which offers explanation for the tiny neutrino mass. The features of extended seesaw mechanism can be realized in this way. Apart from offering the tiny neutrino mass, the extended seesaw model also provides a potentially accessible scale for the RHN mass. The low scale RHN being a feature of this seesaw model serves as an excellent candidate which can explain the source of matter-antimatter asymmetry of the Universe through the process of leptogenesis. There have been plenty of studies which dealt with such low scale leptogenesis from a neutrino mass model embracing the  $U(1)_{B-L}$  symmetry [15]. It is worth mentioning that a low scale seesaw model as embedded in the present framework can also render the gravitino bound harmless [25]. Thus, thermal production of the RHNs do not require too high reheating temperature, protecting the Universe from gravitino overproduction [25]. In addition the extra neutral fermion singlet in this extended seesaw framework facilitates the process of leptogenesis by its self-energy contribution to the final lepton asymmetry to account for the observed baryon asymmetry of the Universe (BAU). This additional self-energy contribution offered by the presence of the extra fermion singlet ( $S$ ) brings an enhancement in the lepton asymmetry which successfully accounts for the observed BAU. We also emphasize on the correlation among the CP violating phases in the neutrino sector with the leptogenesis parameter space.

In another front, the observation of neutrino-less double beta ( $0\nu\beta\beta$ ) decay would prove lepton number violation and the Majorana nature of neutrinos [26], a proper investigation of the said process would be of fundamental importance. Here, we attempt to provide the parameter space in the purview of extended seesaw scenario which is compatible with the constraints related to the  $0\nu\beta\beta$  decay experiments as reported by KamLAND-Zen [27]. Owing to the presence of the neutral fermion singlets we compute the half-life for the potential  $0\nu\beta\beta$  decay process ( $T_{1/2}^{0\nu}$ ). The contribution of the active-sterile mixing to the total  $T_{1/2}^{0\nu}$  of this process has been shown. In this set-up we present an in-depth analysis on the construction of the high energy neutrino mass matrix in the light of an extended seesaw scheme. Although the idea of examining an extended seesaw scheme to investigate for the observed BAU has been conceived before [28], some distinct implications and refinements have not been emphasized earlier. We present the viable parameter space validating this model with

respect to the constraints associated with the neutrino oscillation parameters,  $0\nu\beta\beta$  process and the leptogenesis. In this work we attempt to focus on a detailed analysis on the high energy neutrino mass parameters associated with the said seesaw model along with a low scale leptogenesis in order to offer an explanation for the observed BAU. Most importantly we have shown that, the present framework allows the required amount of lepton asymmetry to put phenomenologically interesting predictions on the neutrino mixing angles mainly the reactor and atmospheric ones, pushing them towards their higher allowed  $3\sigma$  ranges. This fact reinforces the notable features of this analysis. While solving the Boltzmann equations we have dealt with all possible LNV scatterings in order to have a proper investigation on the amount of washout. We carried out a detailed analysis to emphasize the interplay between the generated amount of lepton asymmetry and the corresponding washout.

The outline of this article is as follows. We provide the structure of the model in Section 2, where we brief the light neutrino mass generation through the extended seesaw mechanism. The necessary simulation details required to extract the ESS parameter space along with their numerical estimation are provided in Section 3. Section 4 is dedicated to the necessary prescriptions required for realizing baryogenesis through leptogenesis in the light of the present set-up. We discuss the viable parameter space explaining all the above mentioned BSM issues in Section 5. The constraints associated with  $0\nu\beta\beta$  process are discussed in Section 6. Finally we conclude in Section 7. Additionally for a detailed description of the construction of the extended seesaw mass matrices the analytical algorithm using the seesaw approximation is shown in the Appendix.

## 2 Model description

In this section, we provide a detailed discussion of the model along with theoretical and some experimental constraints on model parameters. We also provide a brief discussion on the generation of neutrino mass in the extended seesaw framework.

### 2.1 Field content and interactions

We extend the Standard Model by an extra  $U(1)_{B-L}$  symmetry. The model contains three right handed neutrinos ( $N_{R_i}$ ) with  $B-L$  charge of  $(-1)$  each as required by anomaly cancellation and three complex singlet sterile neutrinos  $S_{L_i}$ . Apart from this we add two additional scalars  $\chi_1, \chi_2$  which are having  $B-L$  charges as 1 and 2 respectively. The two scalars break the  $U(1)_{B-L}$  symmetry and give mass to the neutrinos. With these two minimal set of singlet scalars we can actually explain the neutrino mass in an extended seesaw set-up. The relevant fields and their respective quantum numbers under the gauge symmetry are shown in table 1.

The Lagrangian for the model can be written as,

$$\mathcal{L} = \mathcal{L}_{\text{SM}} + \mathcal{L}_{\text{gauge}} + \mathcal{L}_{\text{scalar}} + \mathcal{L}_{\text{fermion}}. \quad (2)$$

Firstly, within the  $\mathcal{L}_{\text{SM}}$  itself the gauge fermion interactions will be augmented by new couplings of the SM fermions with the additional  $Z'$  gauge boson coming from the gauged  $U(1)_{B-L}$  symmetry. The kinetic term of the new gauge boson is depicted by the piece  $\mathcal{L}_{\text{gauge}}$ . We are considering here a minimal  $B-L$  extension of the SM and hence the mixing between the  $Z$  and  $Z'$  vanishes [29]. This makes our model simpler and it differs from e.g., [30–32]. The  $\mathcal{L}_{\text{scalar}}$  term takes into account all the scalar (including SM-like Higgs doublet) kinetic and mixing terms. This can be explicitly given as,

$$\mathcal{L}_{\text{scalar}} = (\mathcal{D}_\mu H)^\dagger (\mathcal{D}^\mu H) + (\mathcal{D}_\mu \chi_1)^\dagger (\mathcal{D}^\mu \chi_1) + (\mathcal{D}_\mu \chi_2)^\dagger (\mathcal{D}^\mu \chi_2) + V(H, \chi_1, \chi_2), \quad (3)$$

Fields	$SU(2) \times U(1)_Y$	$U(1)_{B-L}$
$(u_L, d_L)^T$	2,1/3	1/3
$u_R$	1,4/3	1/3
$d_R$	1,-2/3	1/3
$(\nu_L, e_L)^T$	2,-1	-1
$e_R$	1,-2	-1
$H$	2,1	0
$N_{R_i}$	1,0	-1
$S_{L_i}$	1,0	0
$\chi_1$	1,0	1
$\chi_2$	1,0	2

**Table 1:** Fields and their quantum numbers under the gauge symmetry.

where the respective covariant derivatives are given by,

$$\mathcal{D}_\mu H = \partial_\mu H - i g \vec{W}_\mu \cdot \frac{\vec{\tau}}{2} H - i \frac{g'}{2} B_\mu H, \quad (4a)$$

$$\mathcal{D}_\mu \chi_1 = \partial_\mu \chi_1 - i g_{BL} Z'_\mu \chi_2, \quad (4b)$$

$$\mathcal{D}_\mu \chi_2 = \partial_\mu \chi_2 - 2i g_{BL} Z'_\mu \chi_2, \quad (4c)$$

where  $g$ ,  $g'$ , and  $g_{BL}$  are the  $SU(2)_L$ ,  $U(1)_Y$ , and  $U(1)_{B-L}$  couplings, respectively. The  $\vec{W}_\mu$ ,  $B_\mu$ , and  $Z'_\mu$  are the corresponding gauge fields. The most general scalar potential can be written as,

$$\begin{aligned} V(H, \chi_1, \chi_2) = & -\mu_H^2 H^\dagger H + \lambda_H (H^\dagger H)^2 - \mu_1^2 \chi_1^\dagger \chi_1 + \lambda_1 (\chi_1^\dagger \chi_1)^2 - \mu_2^2 \chi_2^\dagger \chi_2 \\ & + \lambda_2 (\chi_2^\dagger \chi_2)^2 + \lambda_{H1} (H^\dagger H) (\chi_1^\dagger \chi_1) + \lambda_{H2} (H^\dagger H) (\chi_2^\dagger \chi_2) \\ & + \lambda_{12} (\chi_1^\dagger \chi_1) (\chi_2^\dagger \chi_2) + [\mu_{12} \chi_2^* \chi_1^2 + \text{H.c.}]. \end{aligned} \quad (5)$$

Here all the  $\mu$ 's are real positive numbers except  $\mu_{12}$ . In order to get a positive mass for  $CP$ -odd scalar states  $\mu_{12}$  has to be negative. The scalars  $\chi_1, \chi_2$  break the  $U(1)_{B-L}$  symmetry and get vacuum expectation values (vev) in this process. The  $SU(2)_L$  doublet scalar  $H$  is involved in usual electroweak symmetry breaking. So we have two phases of symmetry breaking here,

$$SU(2)_L \times U(1)_Y \times U(1)_{B-L} \xrightarrow{\langle \chi_1 \rangle, \langle \chi_2 \rangle} SU(2)_L \times U(1)_Y \xrightarrow{\langle H \rangle} U(1)_{\text{em}}.$$

The fields after the symmetry breaking are written as

$$\chi_1 = \frac{1}{\sqrt{2}}(v_1 + \chi'_1 + i\rho_1), \quad \chi_2 = \frac{1}{\sqrt{2}}(v_2 + \chi'_2 + i\rho_2), \quad H = \frac{1}{\sqrt{2}} \begin{pmatrix} \sqrt{2}\omega^+ \\ v_H + h + i\zeta \end{pmatrix} \quad (6)$$

After the symmetry breaking three  $CP$ -even scalars  $\{h_1, h_2, h_3\}$  will arise out of the mixing of the states  $\{h, \chi'_1, \chi'_2\}$ . Clearly one of  $\{h_1, h_2, h_3\}$  can be identified as the SM-like Higgs. The  $CP$ -odd field  $\zeta$  is absorbed by the  $SU(2)_L$  gauge boson hence is not physical. The other two  $CP$ -odd fields  $\rho_1, \rho_2$  become massive after the symmetry breaking and they mix with each other. From the  $CP$ -odd mass matrix one can confirm that one of the eigenvalues is zero. We can say that the field combination  $\rho_1 \sin \beta + \rho_2 \cos \beta$  ( $\beta$  being the mixing angle between  $\rho_1, \rho_2$ ) is eaten up by the gauge field  $Z'$  and becomes massive, the other combination  $\rho_1 \cos \beta - \rho_2 \sin \beta$  is the only physical  $CP$ -odd field in our model.

Lastly,  $\mathcal{L}_{\text{fermion}}$  in Eq. (2) contains the information of kinetic and Yukawa terms of the BSM fermions and they can be written explicitly as,

$$\mathcal{L}_{\text{fermion}}^{\text{kin}} = \overline{N_{Ri}} i \gamma^\mu (\partial_\mu - i g_{\text{BL}} Z'_\mu) N_{Ri} + \overline{S_{Li}} i \gamma^\mu \partial_\mu S_{Li}, \quad (7)$$

$$-\mathcal{L}_{\text{fermion}}^{\text{Yuk}} = Y_{Dij} \bar{l}_i H (N_R)_j + Y_{Rij} \chi_2^* (N_R)_i^T (N_R)_j + \mu_{ij} (S_L^T)_i (S_L)_j + Y_{Sij} \chi_1^* \bar{N}_{Ri} (S_L)_j + \text{H.c.} \quad (8)$$

here the indices  $i, j$  run from 1-3 and represent the generation indices.

## 2.2 Neutrino Mass generation through extended seesaw mechanism

Owing to the simultaneous presence of both the heavy and small lepton number violating scales  $M_R$  and  $\mu$  respectively, extended seesaw scenario [28] is very different from the inverse seesaw [33–45] and double seesaw scenario [46]. In inverse seesaw mechanism, there is only one small lepton number violating scale  $\mu$  and the lepton number is conserved in the  $\mu = 0$  limit. One of the significant features of this seesaw model is that the presence of the heavy right handed neutrinos do not directly control the generation of the tiny neutrino masses, while playing a crucial role in yielding relatively light sterile neutrinos. Another important characteristic of this extended seesaw mechanism is that, one can have contribution of Majorana neutrinos to  $0\nu\beta\beta$  transition amplitude even in the limit  $\mu \rightarrow 0$ , whereas in the inverse seesaw scenario, the corresponding amplitude vanishes.

One can write the complete neutrino mass matrix which is generated after the symmetry breaking as follows. From Eq. 7 one can derive the neutrino mass matrix as,

$$\mathcal{M}_n = (\nu_L \quad S_L \quad N_R^c) \begin{pmatrix} 0 & 0 & M_D^T \\ 0 & \mu & M_S^T \\ M_D & M_S & M_R \end{pmatrix} \begin{pmatrix} \nu_L^c \\ S_L^c \\ N_R \end{pmatrix}, \quad (9)$$

where the matrix elements are given as:

$$M_D = Y_D v_H, \quad (10)$$

$$M_S = Y_S v_1,$$

$$M_R = Y_R v_2.$$

To the leading order, the light neutrino mass matrix  $m_\nu$ , and the heavy neutrino mass matrices  $m_s, m_R$  can be constructed from the following equations,

$$m_\nu \sim M_D^T (M_S^T)^{-1} \mu (M_S)^{-1} M_D \quad (11)$$

$$m_s \sim \mu - M_S^T M_R^{-1} M_S \quad (12)$$

$$m_R \sim M_R \quad (13)$$

To this end, we refer the reader to Appendix for a detailed construction of the extended seesaw mass matrix following the seesaw parametrization.

## 2.3 Constraints on model parameters

In this section we briefly discuss some of the theoretical and observational constraints on the model parameters.

The boundedness of the scalar potential puts constraints on the respective quartic couplings. Following the method of co-positivity [47, 48], one can easily write down the germane

conditions which in this case are,

$$\lambda_H, \lambda_1, \lambda_2 > 0, \quad (14a)$$

$$\bar{\lambda}_{H1} \equiv \lambda_{H1} + 2\sqrt{\lambda_H \lambda_1} > 0, \quad (14b)$$

$$\bar{\lambda}_{H2} \equiv \lambda_{H2} + 2\sqrt{\lambda_H \lambda_2} > 0, \quad (14c)$$

$$\bar{\lambda}_{12} \equiv \lambda_{12} + 2\sqrt{\lambda_1 \lambda_2} > 0, \quad (14d)$$

$$\lambda_{H1}\sqrt{\lambda_2} + \lambda_{12}\sqrt{\lambda_H} + \lambda_{H2}\sqrt{\lambda_1} + 2\sqrt{\lambda_H \lambda_1 \lambda_2} + \sqrt{2\bar{\lambda}_{H1}\bar{\lambda}_{H2}\bar{\lambda}_{12}} > 0. \quad (14e)$$

The LEP constraint on the ratio of new gauge boson mass to the coupling is [49, 50]

$$\frac{M_{Z'}}{g_{BL}} \geq 6\text{TeV}. \quad (15)$$

Similar bound from ATLAS is quite less stringent  $M_{Z'}/g_{BL} \geq 4.1 \text{ TeV}$  [51].

In the following section we discuss the methodology used to numerically evaluate the allowed parameter space satisfying the neutrino mass and mixing parameters which comply with the  $3\sigma$  global fit presented in table 2.

### 3 Numerical analysis of extended seesaw parameter space

Before discussing the leptogenesis aspects of the model we first consider the constraints on the parameter space coming from the neutrino oscillation data. In this section we describe the methodology used to extract the ranges of the various parameters that can generate the sub-eV light Majorana neutrino mass within the extended seesaw scheme (ESS). As described in the model section the ESS framework is realized by three generations of sterile neutrinos  $S_L$  along with another three generations of heavy right-handed neutrinos  $N_R$ . Thus the high energy neutrino mass matrix basically turns out to be of the dimension  $9 \times 9$ . In order to diagonalize this  $9 \times 9$  mass matrix analytically we follow the procedure given in Refs. [52, 53]. A detailed construction of mass matrices and the corresponding diagonalizing matrices are given in Appendix. We first follow the two steps diagonalization: in the first case we are left with one  $9 \times 9$  block-diagonalized matrix comprising of three  $3 \times 3$  mass matrices:  $m_\nu$ ,  $m_s$  and  $M_R$  for active neutrino and two heavy neutrino states, respectively. The expressions of these mass matrices are provided in Sec. 2.2. The matrices  $\mu$ ,  $M_D$ ,  $M_S$  are considered to be complex symmetric in nature to comply with a non-zero CP phase which can potentially act as a prime source of sizeable lepton asymmetry. However, for simplicity  $M_R$  is chosen to be a real diagonal matrix. This primary choice of the diagonal  $M_R$  also ensures that we are working in a basis of Dirac Yukawa coupling matrix where the RHNs are in their physical mass basis.

For our numerical analysis we vary each elements of the mass matrices in the following ranges (in GeV):

$$10^{-5} \leq \mu \leq 10^{-8} \quad (16)$$

$$10^{-4} \leq M_D \leq 10^{-5} \quad (17)$$

$$0.01 \leq M_S \leq 0.1 \quad (18)$$

whereas,  $M_{R_1}$  and  $M_{R_2}$  are randomly varied from 10 to 20 TeV and are kept to be nearly degenerate in order to make this framework suitable for resonant leptogenesis. The ratio of these two scales is crucial for leptogenesis in the present scenario which we discuss elaborately in the Sec. 4. Following the hierarchy of the RHN mass eigenvalues as  $M_{R_1} \approx M_{R_2} < M_{R_3}$

Parameters	Normal ordering	Inverted ordering
$\sin^2 \theta_{23}$	0.433 - 0.609	0.436 - 0.610
$\sin^2 \theta_{12}$	0.275 - 0.350	0.275 - 0.350
$\sin^2 \theta_{13}$	0.02044 - 0.02435	0.02064 - 0.02457
$\Delta m_{21}^2$	$(6.79 - 8.01) \times 10^{-5} \text{ eV}^2$	$(6.79 - 8.01) \times 10^{-5} \text{ eV}^2$
$\Delta m_{31}^2$	$(2.436 - 2.618) \times 10^{-3} \text{ eV}^2$	$-(2.601 - 2.419) \times 10^{-3} \text{ eV}^2$
$\delta_{CP}/^\circ$	144 - 357	205 - 348

**Table 2:** Latest  $3\sigma$  bounds on the oscillation parameters (With SK data) from Ref. [55].

we proceed for the numerical diagonalization procedure. We keep  $M_{R_3}$  in 50 TeV to 80 TeV range so that it is completely decoupled from other two right-handed neutrinos.

It is evident that working with the  $9 \times 9$  mass matrix with many undetermined parameters may be quite daunting. For our purposes we generate such a large dimensional complete mass matrix numerically for convenience. To simulate this we use `Python` programming which essentially yields the relevant parameter space keeping the constraints on the various mass scales of such ESS framework intact. The complete simulation maintaining neutrino oscillation data as well as desired value of the lepton asymmetry has been performed by in-house `Python 3.8.3` code. From this simulation we obtained parameter points which essentially yield the neutrino oscillation observables. The obtained neutrino mixing parameters are then compared with the current neutrino data pertinent for normal hierarchy (NH), as summarised in table 2. We should mention here that, the present framework is suitable to establish both of the possible neutrino mass hierarchies, however for simplicity and to be in agreement with the recent bias for the NH [54] we only stick to NH of neutrino mass and carry out the analysis relevant for the same. At present the value of Dirac CP phase is ambiguous in the sense that, T2K experiment [56] prefers  $\delta \approx \pi/2$  whereas NOvA [57] tells that  $\delta$  can take CP conserving values. However, the global fit values for each hierarchy imply  $\delta \approx -3\pi/4$  for NH and  $\delta \approx -\pi/2$  for IH as also evident from the table 2. Taking care of the above neutrino oscillation constraints we extract the allowed region of parameter space which we discuss in the following subsection.

### 3.1 ESS parameter space

After constructing the extended seesaw mass matrix numerically ( $\mathcal{M}_n$ ) we diagonalise the same. From the diagonalizing matrix we extract the values of the mixing angles and the CP phases involved in the lepton mixing matrix [58]. fig. 1 evinces a mild correlation among the matrix elements responsible to generate the neutrino observables which comply with experimental data. Here we use different color codes to highlight the required parameter values which are useful for successful leptogenesis. In principle correlations among the neutrino mixing parameters would severely constrain the ESS model parameter space, which may make the model phenomenologically richer. This issue can be well-taken care of if one introduces a flavour symmetry embedded framework which leads to a particular texture of the low energy neutrino mass matrix ( $m_\nu$ ) giving rise to possible correlations among the neutrino observables [12, 59, 60]. In fig. 2 we present the variation of the reactor ( $\theta_{13}$ ) and atmospheric ( $\theta_{23}$ ) mixing angles with respect to the real and imaginary parts of the matrix element of  $M_D$ . It is evident from fig. 2 that the entire range of the ESS parameter space associated with all the matrix elements can yield a non-zero value of  $\theta_{13}$  and  $\theta_{23}$  compatible with the global fit as mentioned in table 2. A similar notion is obtained for the other matrices ( $\mu$  and  $M_S$ ) also, when plotted (not shown here) with respect to these mixing angles of the leptonic mixing

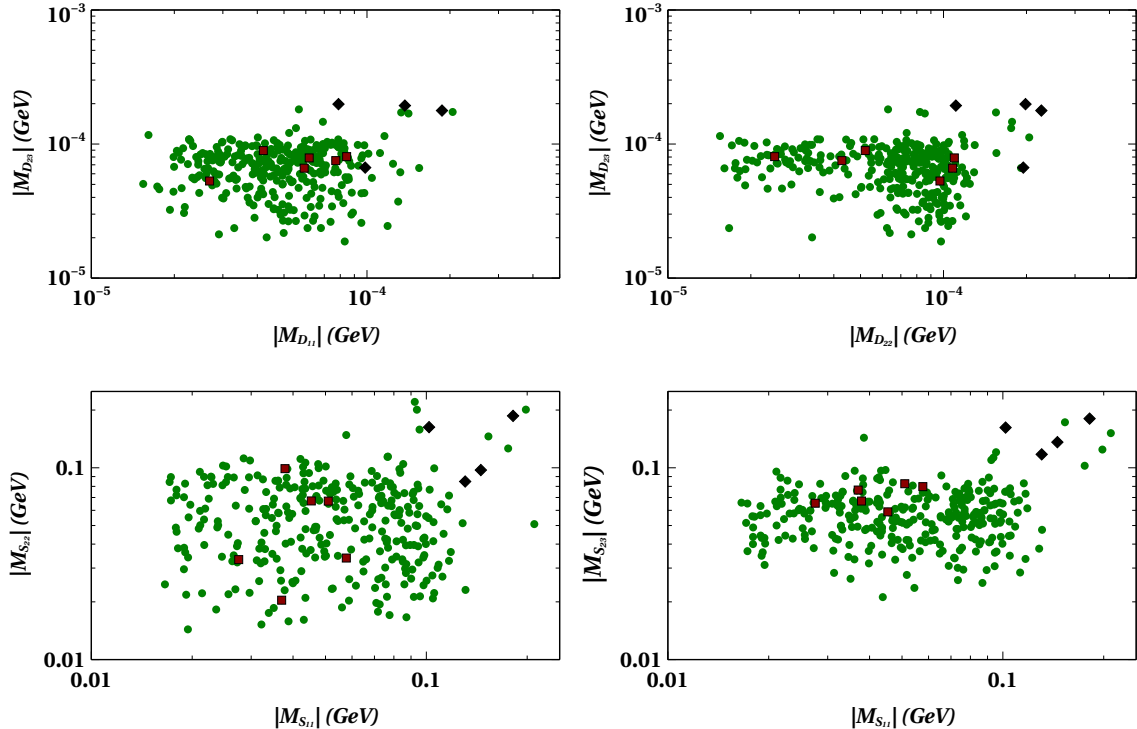


**Figure 1:** Possible correlations among matrix elements. This also shows the constrained parameter space required to have an adequate amount of lepton asymmetry to account for the observed BAU. The red coloured points are identified with the actual data points which can yield  $\eta_B = (2.6 - 6.2) \times 10^{-10}$ . Detailed explanations are provided in the text.

matrix. The red points represent the parameter space which can yield sufficient amount of lepton asymmetry leading to the observed  $\eta_B = (2.6 - 6.2) \times 10^{-10}$ . On the other hand the black points indicate the regions of parameter space which generate ample lepton asymmetry, but can not give rise to the observed  $\eta_B$  due to large amount of washouts associated with them. One can notice from these figures that, in view of successful leptogenesis there exist slight preferences for the higher octant (HO) of the  $\theta_{23}$  and higher values of the  $\theta_{13}$  in its allowed  $3\sigma$  range (shown by the red points). One can understand the breaking of the  $\mu - \tau$  symmetry here by showing the correlations among the mass matrix elements ( $m_{\nu_{ii}}$ , Eq. 11) of the  $\mu - \tau$  sector as presented in fig. 3. Generation of the non-zero reactor angle can be realized by such correlations. We show the variation of the solar ( $\Delta m_{21}^2$ ) and atmospheric ( $\Delta m_{31}^2$ ) neutrino mass splittings as a function of the lightest neutrino mass in fig. 4. Fig. 5 shows the allowed ranges of the heavy and light sterile neutrinos with respect to the lightest active neutrino mass  $m_{\nu_1}$  we obtain in this analysis. It is evident from fig. 4 and fig. 5 that slightly higher values of the lightest active neutrino mass (denoted by red squares) are preferred, owing to the required leptogenesis parameter space. In fig. 6 we present the fourth (active-sterile) mass squared difference ( $\Delta m_{41}^2$ ) as a function of the lightest sterile neutrino mass ( $m_{s_1}$ ) and the active-sterile mixing angle obtained in the set-up. From the right panel of the fig. 6 one can notice the smallness of the active-sterile mixing angle ( $\sin \theta_{14}^2$ ) which mainly oscillate in the range  $10^{-7} - 10^{-5}$ .

Having all the above ESS parameter space, allowed by the neutrino oscillation data, we feed them to lepton asymmetry calculation in order to check for the viable parameter space which can yield the expected baryon to photon ratio ( $\eta_B$ ). The salient features of the various

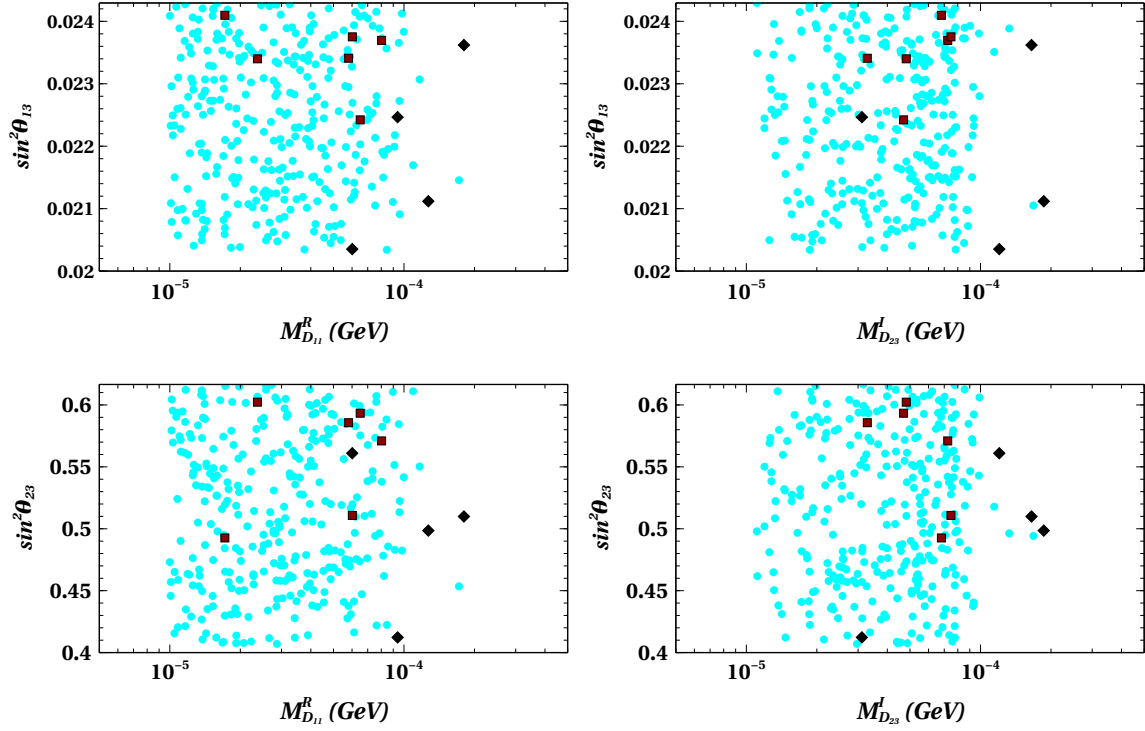


**Figure 2:** Reactor mixing angle ( $\sin^2 \theta_{13}$ ) (upper panel) and atmospheric mixing angle ( $\sin^2 \theta_{23}$ ) (lower panel) as a function of the ESS mass matrix elements. The red points denote the relevant data which can account for the observed BAU. Detailed explanations are in the text.

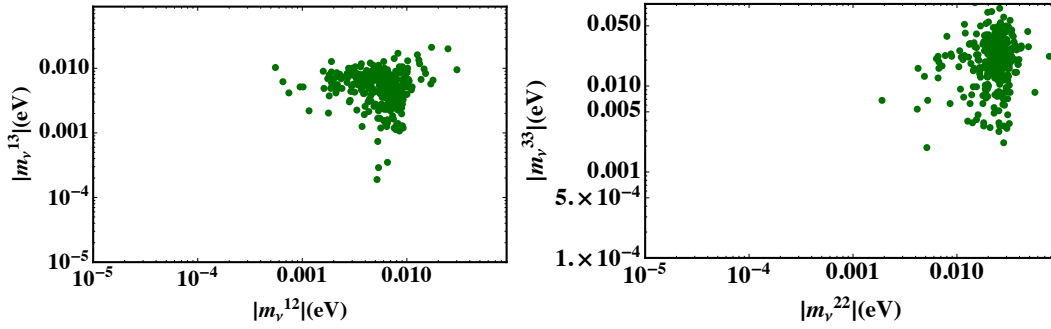


**Figure 3:** Correlation plots among the low energy neutrino mass matrix elements, showing the plane  $m_{e\mu} - m_{e\tau}$  and  $m_{\mu\mu} - m_{\tau\tau}$ .

mass scales (and hence in turn the associated Yukawa couplings) in the context of resonantly enhanced lepton asymmetry will be discussed in the following sections.

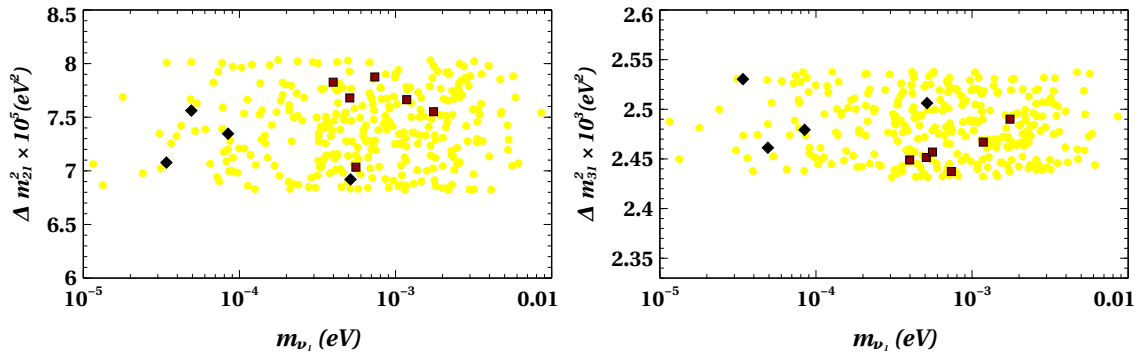


**Figure 4:** Atmospheric and solar neutrino mass squared splittings with respect to the lightest neutrino mass. Red colored squares indicate the relevant data needed to generate an adequate amount of lepton asymmetry. Black colored points are ruled out from the perspective of leptogenesis.

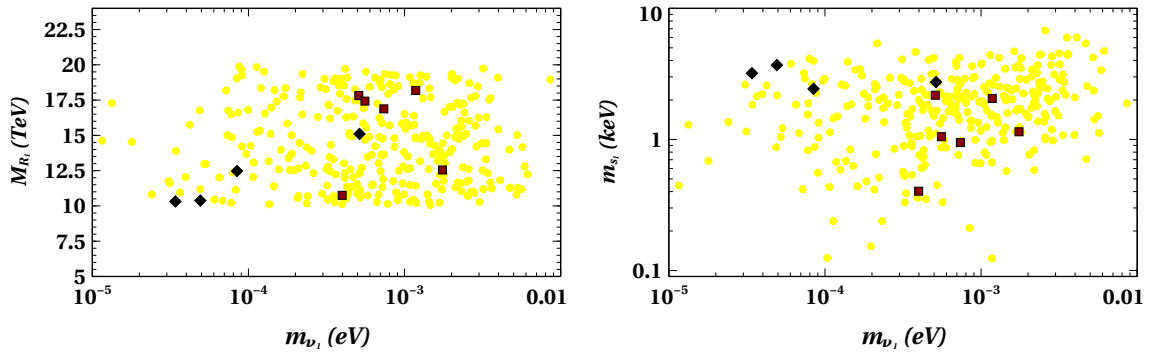


**Figure 5:** Heavy sterile and light sterile masses with respect to lightest Majorana neutrino mass. The choice of the colors can be referred to the same as fig. 4.

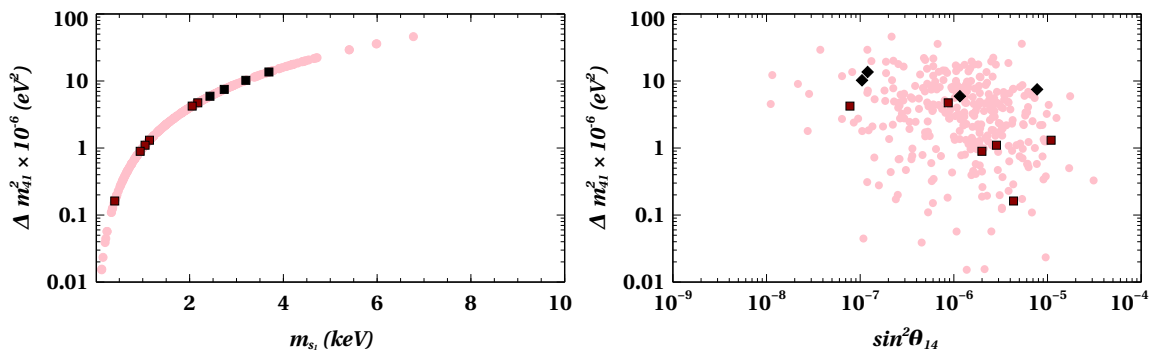


**Figure 6:** Active-sterile mass squared difference as a function of the lightest sterile neutrino mass (left panel) and  $\sin^2 \theta_{14}$  (right panel). The red small squares represent the data which yield ample amount of lepton asymmetry that is responsible for the observed  $\eta_B$ . The black colored rectangles indicate the data points which are ruled out from the need of sufficient leptogenesis.

## 4 Baryogenesis through leptogenesis

### 4.1 Lepton asymmetry parameter

The lepton number asymmetry sourced by the decay of the RHN can be realized as follows

$$\epsilon_i = - \left[ \frac{\Gamma(N_i \rightarrow \bar{l}_i H) - \Gamma(N_i \rightarrow l_i H^*)}{\Gamma(N_i \rightarrow \bar{l}_i H) + \Gamma(N_i \rightarrow l_i H^*)} \right]$$

where,  $N_i$  is the lightest RHN creating the lepton asymmetry. We present the relevant feynmann diagrams for the decay of the lightest RHN in fig 7. It is important to note here that, in this ESS framework the existence of the fourth self-energy diagram participate significantly in bringing out an enhancement of the final lepton asymmetry. We address this issue in detail in the result section of the lepton asymmetry parameter. For massless limit of the final state

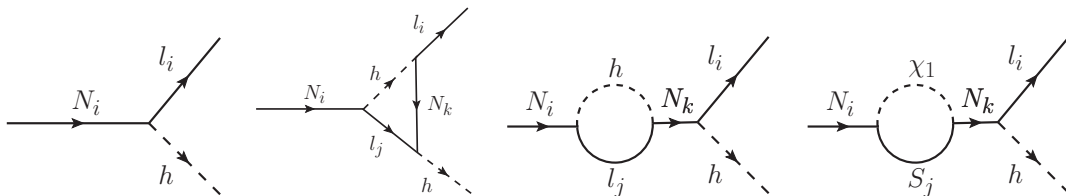


**Figure 7:** Lightest right-handed neutrino decay processes that lead to the lepton asymmetry.

particles of the above decay, the lepton asymmetry can be expressed as [28]

$$\epsilon_1 = \frac{1}{8\pi} \sum_{k \neq 1} ([g_v(x_k) + g_s(x_k)] T_{k1} + g_s(x_k) S_{k1}) \quad (19)$$

with  $T_{k1} = \frac{\text{Im}[(Y_D Y_D^\dagger)_{k1}^2]}{(Y_D Y_D^\dagger + Y_S Y_S^\dagger)_{11}}$  and  $S_{k1} = \frac{\text{Im}[(Y_D Y_D^\dagger)_{k1} (Y_S Y_S^\dagger)_{1k}]}{(Y_D Y_D^\dagger + Y_S Y_S^\dagger)_{11}}$ . The Yanagida loop factors are defined as  $g_v(x) = \sqrt{x_k} (1 - (1+x) \ln \frac{1+x}{x})$  and  $g_s(x) = \frac{\sqrt{x_k}}{1-x_k}$  where,  $x_k = \frac{M_{Rk}^2}{M_{R1}^2}$  for  $k \neq 1$ . As mentioned earlier, a low scale RHN can overcome the gravitino overproduction problem since it requires a smaller reheating temperature. At the same time for a TeV scale RHN being naturally offered by the seesaw scenario under consideration opens up the window to have the leptogenesis taking place through the resonant enhancement of the leptonic asymmetry [22]. Resonant leptogenesis require a very small splitting among the heavy RHN masses of the order of their individual decay width i.e.,  $M_i - M_j \approx \frac{\Gamma_j}{2}$  [22]. In this scenario of large enhancement, the lepton asymmetry can even reach close to unity  $\epsilon_1^l \sim 1$ . Purposefully, we have assumed the heavy right handed Majorana neutrinos  $N_i$  having a quasi degenerate mass spectrum, following  $M_3 > M_1 (\approx M_2)$  so that any two of the three RHNs can contribute in the leptogenesis process. This leads to the realization that studying the evolution of the number density of  $N_1, N_2$  is sufficient in order to obtain their thermal abundance through Boltzmann's equations discussed in the following subsection.

### 4.2 Boltzmann Equations

Solution to the Boltzmann equation 20 provides us with the dynamics of the RHN production and the  $B - L$  number density. From the requirement of producing a lepton asymmetry of the correct order of magnitude, the RHNs have to be numerous before they decay. This essentially relies on the fact that, they are in thermal equilibrium at high temperatures. It is

worth mentioning that we consider here a thermal initial abundance of the RHNs as this can be regarded as a consequence of going through a strong washout regime. The evolutions of number densities of  $N$  and  $B - L$  asymmetry can be obtained by solving the following set of coupled Boltzmann's equations (BEQs) [16, 61]:

$$\frac{dN_{N_i}}{dz} = -D_i(N_{N_i} - N_{N_i}^{eq}), \quad \text{with } i = 1, 2 \quad (20)$$

$$\frac{dN_{B-L}}{dz} = -\sum_{i=1}^3 \epsilon_i D_i (N_{N_i} - N_{N_i}^{eq}) - \sum_{i=1}^3 W_i N_{B-L}, \quad (21)$$

with  $z = \text{Mass of the lightest RHN}/\text{Temperature} = M_{N_i}/T$ , being  $N_i$  as the decaying RHN.  $W_i$  denotes the contribution to the washout term due to inverse decay and  $\Delta L = 2$  scatterings. It is clear from the above set of coupled equations that, one can get the RHN abundance from the first equation and the later determines the  $B - L$  number density which survives in the interplay of the asymmetry production and its washout, with respect to temperature. To ensure the participation of  $N_1, N_2$  in creating the final lepton asymmetry, one has to define a temperature-function ( $z$ ) (for a bit detail one may look into [62]), writing  $z = z_i/\sqrt{x_{1i}}$  with  $i = 1, 2$ . In principle,  $N_{N_i}$ 's are the comoving number densities normalised by the photon density at temperature larger than  $M_{N_i}$ . With the Hubble expansion rate  $H \approx \sqrt{\frac{8\pi^3 g_*}{90}} \frac{M_{N_i}^2}{M_{\text{Pl}}} \frac{1}{z^2} \approx 1.66 g_* \frac{M_{N_i}^2}{M_{\text{Pl}}} \frac{1}{z^2}$  the decay term  $D_i$  in Eq.(20) can be cast into [61],

$$D_i = \frac{\Gamma_{\text{total},i}}{Hz} = K_i x_{1i} z \frac{\mathcal{K}_1(z)}{\mathcal{K}_2(z)}, \quad (22)$$

with  $\Gamma_{\text{total},i}$  as the decay rate of the  $i$ th RHN, and can be expressed as

$$\Gamma_{\text{total},i} = \frac{(Y_D Y_D^\dagger + Y_S Y_S^\dagger)_{ii}}{4\pi} M_{R_i}. \quad (23)$$

In the above Eq. (22)  $\mathcal{K}_1$  and  $\mathcal{K}_2$  mean the modified Bessel functions of the second kind. The washout factor  $K_i$  in Eq.(22) quantifies the deviation of the decay rate of the RHNs from the expansion rate ( $H$ ) of the Universe and can be read as,

$$K_i \equiv \frac{\Gamma_{\text{total},i}}{H(T = M_{N_i})}, \quad (24)$$

One can express the baryon-to-photon ratio with the help of lepton asymmetry as,

$$\eta_B = 0.01 N_{B-L}^{\text{fin}} = 0.01 \epsilon_1 \kappa_1^{\text{fin}} \quad (25)$$

where,  $\kappa_1^{\text{fin}} = \kappa_1(z \rightarrow \infty) < 1$  is the final efficiency factor. The final amount of  $B - L$  asymmetry can also be parametrized as  $Y_{B-L} = n_{B-L}/s$ , where  $s = 2\pi^2 g^* T^3/45$  being the entropy density and  $g^*$  as the effective number of spin-degrees of freedom in thermal equilibrium ( $g^* = 110$ ). After reprocessing by sphaleron transitions, the baryon asymmetry is related to the  $B - L$  asymmetry by [20]  $Y_B = (12/37)(Y_{B-L})$ .

## 5 Results and analysis

### 5.1 Parameter space for leptogenesis

It is important to provide an order of magnitude estimate of the lepton asymmetry obtained with the help of the model parameters that essentially satisfies all the constraints in the

BP V	$Y_{S_{ij}}$	$10^{-6} \begin{pmatrix} 2.08 + 1.79i & 2.26 + 4.26i & 4.58 + 1.80i \\ 2.26 + 4.26i & 1.36 + 3.02i & 4.79 + 4.43i \\ 4.58 + 1.80i & 4.79 + 4.43i & 2.07 + 3.98i \end{pmatrix}$
	$Y_{D_{ij}}$	$10^{-7} \begin{pmatrix} 4.61 + 1.49i & 3.32 + 2.71i & 3.4788 + 1.58i \\ 3.32 + 2.71i & 1.10 + 0.85i & 2.02 + 4.16i \\ 3.47 + 1.58i & 2.02 + 4.16i & 5.48 + 3.86i \end{pmatrix}$
BP IIIa	$Y_{S_{ij}}$	$10^{-6} \begin{pmatrix} 7.36 + 7.03i & 3.93 + 19.395i & 4.75 + 15.28i \\ 3.93 + 19.39i & 12.08 + 10.92i & 10.75 + 12.12i \\ 4.75 + 15.2811i & 10.75 + 12.12i & 15.69 + 6.27i \end{pmatrix}$
	$Y_{D_{ij}}$	$10^{-7} \begin{pmatrix} 7.30 + 2.98i & 3.82 + 5.68i & 6.51 + 3.60i \\ 3.82 + 5.68i & 3.88 + 5.04i & 3.02 + 10.70i \\ 6.51 + 3.60i & 3.02 + 10.70i & 10.10 + 1.78i \end{pmatrix}$

**Table 3:** Numerical estimates of the two Yukawa coupling matrices which correspond to the benchmark values (BP: V and IIIa) presented in table 4.

neutrino sector. As evident from the Eq. (19), there exist essentially two different sets of Yukawa couplings namely  $(Y_D, Y_S)$ , which determine the order of the lepton asymmetry one should get in this ESS framework. These two complex Yukawa couplings are the sources of lepton asymmetry in the present scenario. We show the role of these complex coupling coefficients in the form of the corresponding matrix elements in obtaining the correct order of lepton asymmetry  $\epsilon$  in fig. 8, and fig. 9. These two figures emphasize on the choices of Yukawa couplings and in turn the ESS parameter space in order to make this framework suitable for leptogenesis. For this purpose different color codes have been used to highlight the ESS parameter spaces that are essentially required to be chosen (by dark red square) and omitted (by black diamond). It is important here to note from the expression of the lepton asymmetry (Eq. (19)) that, the large Yukawa coupling  $Y_S$  plays a vital role in bringing the order of lepton asymmetry even up to around  $10^{-3}$  for a considerably large region of the entire parameter space of ESS. In addition to this, we would like to emphasize on the fact that, despite of this large  $Y_S$  the criteria satisfying  $|M_i - M_j| \sim \frac{\Gamma_j}{2}$  is unavoidable even after the presence of an additional self-energy diagram in the present set-up. This is guided by keeping a quasi-degenerate RHN mass spectrum for instance  $M_1 \approx M_2 < M_3$ . Thereafter, we consider the decay of more than one RHN and have noticed that the generated asymmetry is solely dependent on the lightest heavy RHN ( $N_1$  here), even if the second RHN ( $N_2$ ) is not having pronounced mass hierarchy with the former. For a clear understanding of this fact one may refer to table 4. In fig. 8 we show the variation of the lepton asymmetry as a function of the matrix elements  $M_D$ . The reliance of the lepton asymmetry on the  $M_S$  matrix elements have been shown in fig. 9. This is also evident from the table 3, where we present the Yukawa couplings for the particular benchmark value of the lepton asymmetry parameter. Presented data in the table 4 leads to the realization that in this ESS scenario one has to be very careful while choosing the texture of Yukawa coupling matrices, as it is evident that even after having a large magnitude of lepton asymmetry one can not reproduce the observed baryon to photon ratio since the associated washouts corresponding to those Yukawa couplings are large enough to erase a considerable part of the generated lepton asymmetry. It will be more transparent if one notices the data provided for BP-IIIa in the table 4. The large washout restricts the parameter spaces for the Yukawa couplings in order to have a successful leptogenesis.

In fig. 10 we present the dependence of lepton asymmetry on the low energy parameters and also on the RHN mass splitting  $\Delta M = M_{R_2} - M_{R_1}$ . As it is seen from the left panel of fig. 10 that the largest asymmetry is obtained for the sum over neutrino mass to fall around  $0.06 \text{ eV}$ . The amount of the washout we get in this scenario turns to be of the order of  $10^{2,3}$

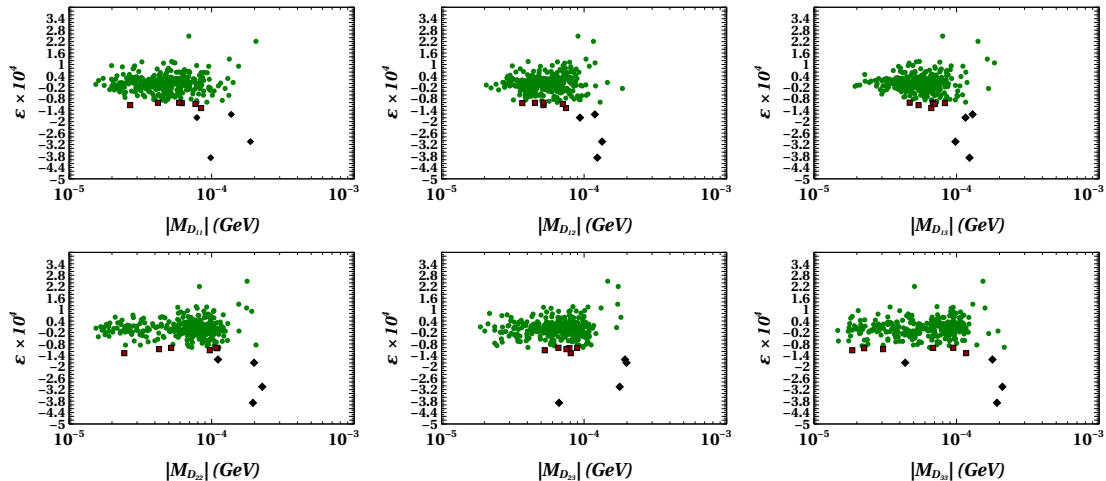


**Figure 8:** Lepton asymmetry versus matrix elements of  $M_D$ . The red squares are identified with the appropriate parameter space which is essential for a successful leptogenesis. The black color indicates those parameter spaces which after having an adequate lepton asymmetry can not successfully account for the observed  $\eta_B$ .

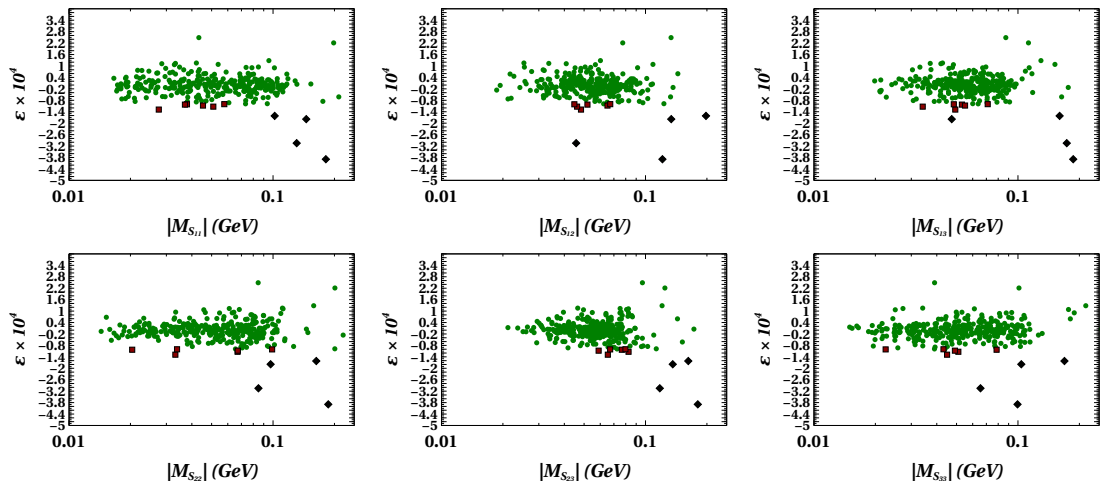


**Figure 9:** Lepton asymmetry versus matrix elements of  $M_S$ . To have an idea about the various colored data points one can refer to the caption of fig. 8.

which is in agreement with the situation one has to go through while having a resonantly enhanced lepton asymmetry. As mentioned earlier, to have a proper treatment of all the washout processes we also calculate the contributions from various  $2 \rightarrow 2$  LNV scattering processes that enter the Boltzmann equations. The final  $B - L$  asymmetry which remained in the interplay of creation of the asymmetry and its washout through various concerned processes are presented in fig. 11. In the right panel of fig. 11 we present the  $B - L$  evolutions with respect to the temperature function for different values of lepton asymmetry which are large in number. One can notice from this figure that, even after having a large amount of lepton asymmetry we may not generate the required amount of  $B - L$  charge if the corresponding washouts erase a part of the asymmetry leading to a decrease in the final baryon asymmetry. This fact can also be well-understood from the table 4.

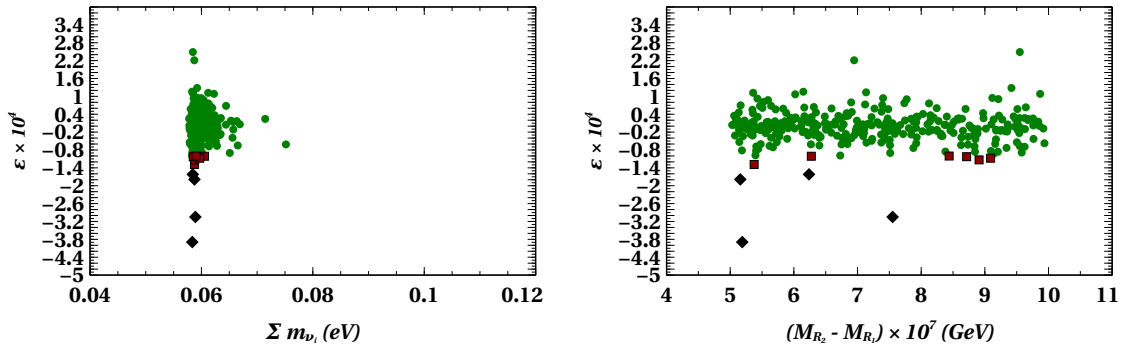


**Figure 10:** Lepton asymmetry as a function of  $\sum m_{\nu_i}$  and the RHN mass splitting  $M_{R_2} - M_{R_1}$ .

BP	$K_1$	$K_2$	$ \epsilon_1 $	$ \epsilon_2 $	$\eta_B$
I	414.62	272.60	$9.52 \times 10^{-7}$	$2.32 \times 10^{-15}$	$2.16 \times 10^{-12}$
II	498.9	233.85	$8.3 \times 10^{-6}$	$2.05 \times 10^{-15}$	$1.7 \times 10^{-11}$
III(a)	3311.41	4052.22	$1.61 \times 10^{-4}$	$8.01 \times 10^{-15}$	$2.77 \times 10^{-11}$
III(b)	2199.18	2452.32	$1.78 \times 10^{-4}$	$2.22 \times 10^{-15}$	$5.04 \times 10^{-11}$
III(c)	4362.4	4343.9	$3.89 \times 10^{-4}$	$5.95 \times 10^{-15}$	$5.57 \times 10^{-11}$
III(d)	1795.48	850.57	$3.04 \times 10^{-4}$	$2.85 \times 10^{-15}$	$1.9 \times 10^{-10}$
IV	182.15	415.42	$1.13 \times 10^{-4}$	$1.18 \times 10^{-15}$	$3.003 \times 10^{-10}$
V	284.47	395.30	$1.28 \times 10^{-4}$	$2.05 \times 10^{-15}$	$2.95 \times 10^{-10}$

**Table 4:** Bench mark values for the lepton asymmetry parameters and the corresponding washout amount which altogether yield the final baryon to photon ratio ( $\eta_B$ ). These  $\eta_B$  values are evaluated at  $z = 100$  from the solution of the Boltzmann Equations.

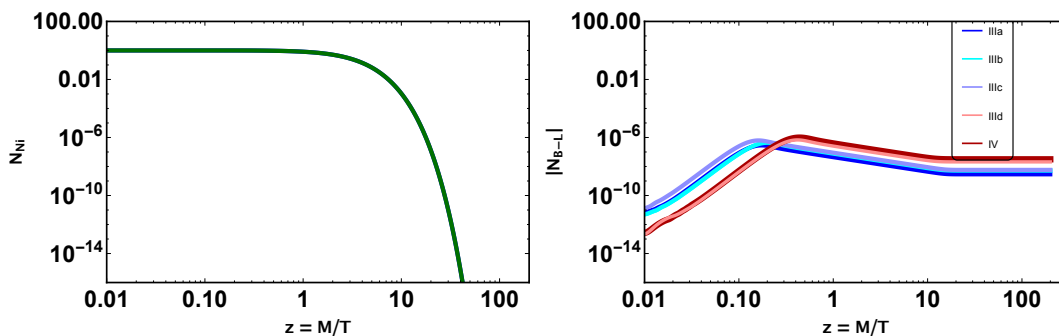


**Figure 11:** RHN abundance (left panel) and  $B - L$  abundance (right panel). Various colors in the second figure represent the final  $B - L$  production amount out of each case with different amounts of lepton asymmetries and corresponding washouts, identified with the benchmark points as tabulated in table 4.

## 6 Neutrinoless double beta decay

Neutrinoless double beta decay ( $0\nu\beta\beta$ ) is a lepton number violating process, which, if observed, would establish the Majorana nature of neutrinos with certainty [63–66]. In various beyond SM scenarios the rate of this process can get enhancement and become observable

in experiments [66–68]. The dominant contribution to the  $0\nu\beta\beta$ -decay rate,  $\Gamma_{0\nu}$ , is due to the exchange of three light Majorana neutrinos  $\nu_i$  [69]. However it is customary to look for other contributions to the final process owing to the presence of extra particle species that can mediate the said process. In ESS, additional sterile neutrinos can play important role. To this end, along with the light Majorana neutrinos  $\nu_i$ , the right-handed (RH) neutrino states  $N_{R_i}$  for ( $i = 1, 2, 3$ ) and  $S_{L_j}$  for ( $j = 1, 2, 3$ ) can also mediate  $0\nu\beta\beta$  process  $2n \rightarrow 2p + 2e^-$ . Due to its heavier mass the contribution of  $N_{R_i}$  to the final amplitude of the  $0\nu\beta\beta$  process will be suppressed enough, as the strength of this particular channel will be determined by the mixing of active neutrino states with the heavy sterile ( $V_{eN_i}$ ). Additionally, the contribution will be suppressed by the heavy sterile mass  $M_{R_i}$ . The  $V_{eN}$  is given by  $M_D^\dagger M_R^{-1} W_N$  (see Eq. 61) where  $W_N$  is defined as diagonalization matrix of heavy sterile states given in Eq. 57. The contribution from the  $0\nu\beta\beta$  channel mediated by the heavy sterile neutrino can be expressed by

$$\mathcal{A}_N \sim \frac{V_{eN_i}^2}{M_{R_i}} \quad (26)$$

where  $V_{eN_i}$  is the mixing of active neutrinos with the  $N_{R_i}$  states.

On the other hand the amplitude of the  $0\nu\beta\beta$  process, mediated by the comparatively light sterile neutrino states  $S_{L_i}$  for  $m_{s_i} > \langle p^2 \rangle^1$  can be expressed as

$$\mathcal{A}_S \sim \frac{V_{eS_i}^2}{m_{s_i}}, \quad (27)$$

with  $V_{eS_i}$  being the mixing between the active neutrino with the sterile neutrino given by  $M_D^\dagger M_S^{-1} W_s$  in the present framework, whereas, for  $m_{s_i} < \langle p^2 \rangle$

$$\mathcal{A}_S \sim \frac{V_{eS_i}^2 m_{s_i}}{\langle p^2 \rangle} \quad (28)$$

One can write the simplified expression for the amplitude, taking simultaneously into account  $\langle p^2 \rangle \simeq m_{s_i}^2 \simeq 100 - 200 \text{ MeV}^2$ .

$$\mathcal{A}_S \sim \frac{V_{eS_i}^2 m_{s_i}}{\langle p^2 \rangle - m_{s_i}^2}. \quad (29)$$

The half-life of  $0\nu\beta\beta$  is given by

$$\left(T_{1/2}^{0\nu}\right)^{-1} = K_{0\nu} \left| \frac{U_{ei}^2 m_{\nu_i}}{\langle p^2 \rangle - m_{\nu_i}^2} + \frac{V_{eS_i}^2 m_{s_i}}{\langle p^2 \rangle - m_{s_i}^2} + \frac{V_{eN_i}^2 M_{R_i}}{\langle p^2 \rangle - M_{R_i}^2} \right|^2. \quad (30)$$

where,  $i$  implies for all the light and heavy neutrino states, supposed to mediate the potential  $0\nu\beta\beta$  process. The details of the notation and convention can be found in Appendix. In the above, we also have  $K_{0\nu} = G_{0\nu} (\mathcal{M}_N m_p)^2$  and  $\langle p^2 \rangle \equiv -m_e m_p \frac{\mathcal{M}_N}{\mathcal{M}_\nu}$ . Here  $G_{0\nu}$  is the phase space factor,  $M_N$  is the nuclear matrix element (NME) for heavy sterile exchange whereas  $M_\nu$  is the corresponding element for light sterile exchange. The required values of  $G_{0\nu}$  and NMEs have been taken from Ref. [70]. In our analysis, we stick to particular values of NMEs as  $\mathcal{M}_N = 163.5$  and  $\mathcal{M}_\nu = 2.29$ ; and the phase space factor  $G_{0\nu}$  is  $5.92 \times 10^{-14} \text{ year}^{-1}$ . For completeness we focus on the contribution of the lighter sterile neutrino states  $S_L$ . As mentioned earlier, the heavier states ( $N_R$ ), being considerably heavier  $10^4 - 10^5 \text{ GeV}$  and having the active-sterile mixing  $\sim M_D/M_R \sim 10^{-10} - 10^{-8}$  give negligible contribution in

---

<sup>1</sup>We shall define it shortly.

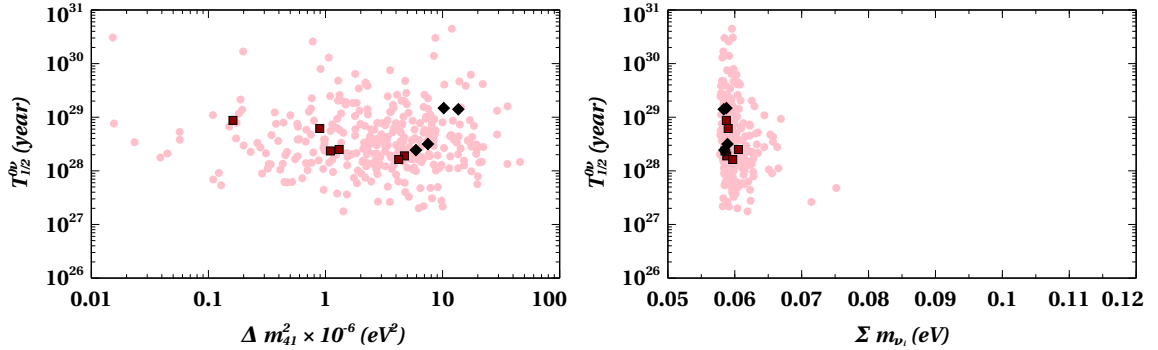


**Figure 12:** Prediction for the half-life of the  $0\nu\beta\beta$  process as a function of the fourth mass squared splittings  $\Delta m_{41}^2$  (left) and sum over neutrino masses (right). The reason behind the choice of different colors can be obtained from the caption of fig. 6. Here the values of nuclear matrix elements (NMEs) are  $\mathcal{M}_N = 163.5$  and  $\mathcal{M}_\nu = 2.29$ ; the phase space factor  $G_{0\nu}$  is taken as  $5.92 \times 10^{-14} \text{ year}^{-1}$  [70].

$0\nu\beta\beta$ . On the other side there seems to be sizeable contribution from the the lighter sterile neutrino states to the final amplitude of  $0\nu\beta\beta$  process, due to the larger active-sterile mixing  $V_{eS}$ . It is to note that to keep some window open for keV sterile dark matter candidate, the mass window for the lighter sterile state has been chosen to be around keV to a few MeV.

The theoretical prediction on the  $T_{1/2}^{0\nu}$  drawn from the constraints of this framework, has been compared with the one reported by recent KamLAND-Zen experiment which sets  $T_{1/2}^{0\nu} > 1.07 \times 10^{26} \text{ year}$  [27, 71]. Till date the best lower limit on the half-life of the  $0\nu\beta\beta$  using  $^{76}\text{Ge}$  is  $T_{1/2}^{0\nu} > 8.0 \times 10^{25} \text{ yrs}$  at 90% C.L. from GERDA [72]. The proposed sensitivity of the future planned nEXO experiment is  $T_{1/2}^{0\nu} \approx 6.6 \times 10^{27} \text{ yrs}$  [73]. Though we do not have any direct experimental proof for  $0\nu\beta\beta$  transition [74–82] the search for improving the bound on the  $T_{1/2}^{0\nu}$  value is still beneficial to explore the possibility of new physics [77, 81, 83–89].

The theoretical prediction of the  $T_{1/2}^{0\nu}$  value in the ESS framework is shown in fig. 12. It is expressed as functions of square of mass splitting of  $S_1$  and active electron neutrino and also as function of sum over active neutrino masses  $\Sigma m_{\nu_i}$ . It is evident from the figure that all points are allowed from the limit set by KamLAND-Zen experiment [27].

## 7 Conclusion

We present a standard model extension augmented by a  $U(1)_{B-L}$  symmetry to offer an explanation to the light Majorana neutrino mass as well as the observed matter-antimatter asymmetry of the Universe through a low scale seesaw model. Our study is stimulated by the requirement of having a TeV scale RHN along with a potential dark matter candidate which is of astrophysical significance. In this work we have systematically investigated the viable parameter space of an extended seesaw framework to meet the observed matter-antimatter asymmetry. Having the ESS framework leads to the realization that the presence of the additional sterile neutrino generations takes a strong hold in the lepton asymmetry parameter space through an extra self-energy contribution. We have emphasized here the new findings which are the prime requirements in order to account for a successful leptogenesis in this ESS framework in the context of the work done by the authors in Ref. [28]. We present the key findings of our analysis below.

The model parameter space arising from this ESS scheme can explain both the hierarchies of neutrino mass pattern. We have presented mild correlations among the mass matrix elements, which further can explain the properties of the leptonic mixing matrix. In particular it is worth-mentioning that, the allowed parameter space for successful leptogenesis in this ESS model brings out rich predictions on the low energy neutrino mixing data. In the context of leptogenesis we obtained significant preferences in the neutrino observables for the octant of the atmospheric mixing angle ( $\theta_{23} > 45^\circ$ ) along with the reactor mixing angle ( $\theta_{13} > 8.52^\circ$ ). These low energy predictions for mixing angles make this framework a viable scenario to be tested from the perspective of future and ongoing neutrino oscillation experiments. This model predicts the entire  $3\sigma$  range for the Dirac CP phase  $\delta$ . The sum over neutrino mass obtained from this analysis ( $\sum m_i < 0.12$  eV) is found to be well within the bound reported by Cosmology. We also briefly address on how the model parameter space impacts the half-life period of the  $0\nu\beta\beta$  decay process ( $T_{1/2}^{0\nu} > 10^{27}$  yrs) which is in agreement with the half-life period as envisaged by the recent KamLAND-Zen experiment.

In the later part, we have discussed how the resulting complex Yukawa coupling matrices play their role in realizing baryogenesis through leptogenesis scenario by the CP-violating decay of TeV scale RHN. We keep the RHN mass window to be around 10-20 TeV. It is worth mentioning that in spite of having an additional self-energy contribution to the lepton asymmetry, the tiny splitting among the RHN masses is unavoidable which is a basic criteria of facing resonant leptogenesis. The washout in this framework strictly hints towards a strong washout regime, which is also approved by the low energy neutrino data. The highest and ample amount of lepton asymmetry we report here to be around  $1.13 \times 10^{-4}$ . We also observe here that although for some parameter space of ESS we obtain a large amount of lepton asymmetry, the final baryon asymmetry gets depleted by a factor due to the large washout.

The present analysis confers a detailed construction of the extended seesaw parameter space. It is interesting to note that within the allowed seesaw parameter space satisfying the neutrino oscillation data, only some particular regions can actually account for a sufficient amount of lepton asymmetry which has to be of around  $10^{-4}$ . Thus it is worth mentioning that this particular extension of the canonical seesaw model play a crucial role in obtaining an enhanced lepton asymmetry which translates into the requirement for the cosmological baryon asymmetry of the Universe both from the quantitative and the qualitative point of view. This model can potentially manifest its signatures in search of TeV scale Majorana right handed neutrino in the future collider searches. An added bonus of this model is the existence of a keV sterile neutrino which can also play the role of a non-thermal dark matter candidate, the detailed phenomenological study of which we keep for a forthcoming work.

## Acknowledgement

UKD acknowledges the support from Department of Science and Technology (DST), Government of India under the grant reference no. SRG/2020/000283. TJ thanks Ram Lal Awasthi, Sarif Khan, Amina Khatun and Soumya C for important discussions. TJ acknowledges the facilities provided by Institute of Physics, Bhubaneswar as the collaboration was started during the stay at IOP. TJ also acknowledges Adrish Maity, Saptarshi Mukherjee and Tapolina Jha for important discussion regarding the computational part. Authors also acknowledge them as a part of the simulation has been performed using their machine at initial stage of the work. Authors acknowledge the HPC facility (Vikram-100 HPC) provided by PRL, Ahmedabad. AM also wants to thank Ashimananda Modak for useful discussion related to numerical simulation. NS acknowledges RUSA 2.0 Project.

## Appendix

Here we briefly explain the diagonalization procedure in extended seesaw framework for completeness. This is largely based on the method outlined in [52, 53]. The neutral mass matrix  $\mathcal{M}_n$  is given by

$$\mathcal{M}_n = \begin{pmatrix} 0 & 0 & M_D^T \\ 0 & \mu & M_S^T \\ M_D & M_S & M_R \end{pmatrix}. \quad (31)$$

In the entire analysis, we consider Majorana matrix  $M_R$  to be real and diagonal. The  $\mu$  being another Majorana mass matrix is considered to be complex symmetric. The Dirac mass matrices  $M_S, M_D$  are also complex symmetric matrices. The matrix  $\mathcal{M}_n$  can be block-diagonalized as  $\mathcal{U}_1^T \mathcal{M}_n \mathcal{U}_1 = \mathcal{M}_{bd}$  where,  $\mathcal{U}_1$  and  $\mathcal{M}_{bd}$  are the final block-diagonalization matrix and final block-diagonal mass matrix respectively. Furthermore,  $\mathcal{U}_1$  can be decomposed as  $\mathcal{U}_1 = \mathcal{U}'_1 \mathcal{U}''_1$ . So, we have  $\mathcal{U}'_1{}^T \mathcal{M}_n \mathcal{U}'_1 = \hat{\mathcal{M}}_{bd}$  followed by another block-diagonalization as  $\mathcal{U}''_1{}^T \hat{\mathcal{M}}_{bd} \mathcal{U}''_1 = \mathcal{M}_{bd}$ , with  $\hat{\mathcal{M}}_{bd}$  being the intermediate block-diagonalization matrix. We follow the parametrization of Ref. [52], *i.e.*,

$$\mathcal{U}'_1 = \begin{pmatrix} \sqrt{\mathbb{1}_{2 \times 2} - \mathcal{B}\mathcal{B}^\dagger} & \mathcal{B}_{2 \times 1} \\ -\mathcal{B}^\dagger_{1 \times 2} & \sqrt{\mathbb{1}_{1 \times 1} - \mathcal{B}^\dagger \mathcal{B}} \end{pmatrix}, \quad (32)$$

where,  $\mathcal{B} = \begin{pmatrix} \mathcal{B}_{aa} \\ \mathcal{B}_{bb} \end{pmatrix}$ ,  $\mathcal{B} = \mathcal{B}_1 + \mathcal{B}_2 + \mathcal{B}_3 + \dots$  and  $\sqrt{1 - \mathcal{B}\mathcal{B}^\dagger} = 1 - \frac{1}{2}\mathcal{B}_1\mathcal{B}_1^\dagger - \frac{1}{2}(\mathcal{B}_1\mathcal{B}_2^\dagger + \mathcal{B}_2\mathcal{B}_1^\dagger) - \frac{1}{2}(\mathcal{B}_1\mathcal{B}_3^\dagger + \mathcal{B}_2\mathcal{B}_2^\dagger + \mathcal{B}_3\mathcal{B}_1^\dagger + \frac{1}{4}\mathcal{B}_1\mathcal{B}_1^\dagger\mathcal{B}_1\mathcal{B}_1^\dagger) + \dots$ ; so,  $\mathcal{B}_{aa \setminus bb} = \mathcal{B}_{aa1 \setminus bb1} + \mathcal{B}_{aa2 \setminus bb2} + \mathcal{B}_{aa3 \setminus bb3} + \dots$ . From the following diagonalization (block)

$$\mathcal{U}'_1{}^T \mathcal{M}_n \mathcal{U}'_1 = \hat{\mathcal{M}}_{bd} = \begin{pmatrix} \mathcal{M}_{\text{light}_{2 \times 2}} & \mathbb{0}_{2 \times 1} \\ \mathbb{0}_{1 \times 2} & \mathcal{M}_{\text{heavy}_{1 \times 1}} \end{pmatrix}, \quad (33)$$

we get,

$$\mathcal{B}^T \widetilde{M}_L \sqrt{1 - \mathcal{B}\mathcal{B}^\dagger} - \mathcal{B}^T \widetilde{M}_D^T \mathcal{B}^\dagger + \sqrt{1 - \mathcal{B}^T \mathcal{B}^*} \widetilde{M}_D \sqrt{1 - \mathcal{B}\mathcal{B}^\dagger} - \sqrt{1 - \mathcal{B}^T \mathcal{B}^*} M_R \mathcal{B}^\dagger = 0, \quad (34)$$

where,  $\widetilde{M}_L = \begin{pmatrix} 0 & 0 \\ 0 & \mu \end{pmatrix}$  and  $\widetilde{M}_D = (M_D \quad M_S)$ .

Considering  $\mathcal{B}_j \propto \frac{1}{M_R^j}$  and equating different coefficients of  $M_R^j$  for different values of  $j$  from the above equation:

$$M_R \mathcal{B}_1^\dagger = \widetilde{M}_D, \quad (35)$$

$$M_R \mathcal{B}_2^\dagger = M_R^{-1*} \widetilde{M}_D^* \widetilde{M}_L. \quad (36)$$

Solving above equations we get,

$$\mathcal{B}_{aa1} = M_D^\dagger M_R^{-1}, \quad \mathcal{B}_{bb1} = M_S^\dagger M_R^{-1}, \quad \mathcal{B}_{aa2} = 0, \quad \mathcal{B}_{bb2} = \mu^* M_S^T M_R^{-2}. \quad (37)$$

So, the block-diagonalized mass matrices

$$\begin{aligned} \mathcal{M}_{\text{light}_{2 \times 2}} &= \widetilde{M}_L - \frac{1}{2}(\mathcal{B}_1^* \mathcal{B}_1^T \widetilde{M}_L + \widetilde{M}_L \mathcal{B}_1 \mathcal{B}_1^\dagger) - \widetilde{M}_D^T (\mathcal{B}_1^\dagger + \mathcal{B}_2^\dagger) + \mathcal{B}_1^* M_R \mathcal{B}_1^\dagger \\ &= \begin{pmatrix} -M_D^T M_R^{-1} M_D & -M_D^T M_R^{-1} M_S - \frac{1}{2} M_D^T M_R^{-2} M_S^* \mu \\ -M_S^T M_R^{-1} M_D - \frac{1}{2} \mu M_S^\dagger M_R^{-2} M_D & \mu - M_S^T M_R^{-1} M_S - \frac{1}{2} (M_S^T M_R^{-2} M_S^* \mu + \mu M_S^\dagger M_R^{-2} M_D) \end{pmatrix}. \end{aligned} \quad (38)$$

and,

$$\begin{aligned}
\mathcal{M}_{\text{heavy}_{1 \times 1}} &= M_R + \mathcal{B}_1^T \widetilde{M}_L \mathcal{B}_1 + \frac{1}{2} \widetilde{M}_D \mathcal{B}_1 + \frac{1}{2} \widetilde{M}_D \mathcal{B}_2 + \mathcal{B}_1^T \widetilde{M}_D^T + \mathcal{B}_2^T \widetilde{M}_D^T \\
&\quad - \frac{1}{2} M_R \mathcal{B}_2^\dagger \mathcal{B}_1 - \frac{1}{2} \mathcal{B}_1^T \mathcal{B}_1^* M_R - \frac{1}{2} \mathcal{B}_1^T \mathcal{B}_2^* M_R - \frac{1}{2} \mathcal{B}_2^T \mathcal{B}_1^* M_R \\
\Rightarrow M'_R &= M_R + \frac{1}{2} (M_D M_D^\dagger M_R^{-1} + M_S M_S^\dagger M_R^{-1} + M_R^{-1} M_D^T M_D^T + M_R^{-1} M_S^* M_S^T) \\
&\quad + \frac{1}{2} (M_S \mu^* M_S^T M_R^{-2} + M_R^{-2} M_S \mu^* M_S^T) \\
\Rightarrow M'_R &= M_R + \frac{1}{2} [(M_D M_D^\dagger + M_S M_S^\dagger) M_R^{-1} + M_S \mu^* M_S^T M_R^{-2} + \text{Trans.}] \simeq M_R.
\end{aligned} \tag{39}$$

Substituting the values of  $\mathcal{B}$  from Eq. (37) to Eq. (32) and considering expansion up to  $M_R^{-1}$  we get,

$$\mathcal{U}'_1 = \begin{pmatrix} 1 - \frac{1}{2} M_D^\dagger M_R^{-2} M_D & -\frac{1}{2} M_D^\dagger M_R^{-2} M_S & M_D^\dagger M_R^{-1} \\ -\frac{1}{2} M_S^\dagger M_R^{-2} M_D & 1 - \frac{1}{2} M_S^\dagger M_R^{-2} M_S & M_S^\dagger M_R^{-1} + \mu^* M_S^T M_R^{-2} \\ -M_R^{-1} M_D & -(M_R^{-1} M_S + M_R^{-2} M_S^* \mu) & 1 - \frac{1}{2} M_R^{-1} (M_D M_D^\dagger + M_S M_S^\dagger) M_R^{-1} \end{pmatrix}. \tag{40}$$

Using the expressions of Eqs. (39) and (38) (neglecting powers lower than  $M_R^{-1}$ ) we have the intermediate block diagonalization matrix as

$$\hat{\mathcal{M}}_{bd} = \begin{pmatrix} -M_D^T M_R^{-1} M_D & -M_D^T M_R^{-1} M_S & 0 \\ -M_S^T M_R^{-1} M_D & \mu - M_S^T M_R^{-1} M_S & 0 \\ 0 & 0 & M_R \end{pmatrix}. \tag{41}$$

For further block-diagonalization, we again follow the same prescriptions [52, 53]. Following the similar *ansatz*, we have,

$$\mathcal{U}''_1 = \begin{pmatrix} \sqrt{1 - \mathcal{B}' \mathcal{B}'^\dagger} & \mathcal{B}' \\ -\mathcal{B}'^\dagger & \sqrt{1 - \mathcal{B}'^\dagger \mathcal{B}'} \end{pmatrix}, \tag{42}$$

and from similar diagonalization

$$\mathcal{U}_1''^T \hat{\mathcal{M}}_{bd} \mathcal{U}_1'' = \mathcal{M}_{bd} = \begin{pmatrix} \mathcal{M}_{\text{light}} & 0 \\ 0 & \mathcal{M}_{\text{heavy}} \end{pmatrix}, \tag{43}$$

we obtain

$$\begin{aligned}
&\mathcal{B}'^T (-M_D^T M_R^{-1} M_D) \sqrt{1 - \mathcal{B}' \mathcal{B}'^\dagger} - \mathcal{B}'^T (-M_D^T M_R^{-1} M_S) \mathcal{B}'^\dagger \\
&+ \sqrt{1 - \mathcal{B}'^T \mathcal{B}'^*} (-M_S^T M_R^{-1} M_D) \sqrt{1 - \mathcal{B}' \mathcal{B}'^\dagger} - \sqrt{1 - \mathcal{B}'^T \mathcal{B}'^*} (\mu - M_S^T M_R^{-1} M_S) \mathcal{B}'^\dagger = 0.
\end{aligned} \tag{44}$$

Assuming  $\mathcal{B}'_j \propto \frac{1}{M_S^j}$ , expressions of different  $\mathcal{B}'$  can be obtained by equating different coefficients of  $M_S^j$  for different values of  $j$  from Eq. 44:

$$-M_S^T M_R^{-1} M_D + M_S^T M_R^{-1} M_S \mathcal{B}'_1{}^\dagger = 0, \tag{45}$$

$$M_S^T M_R^{-1} M_S \mathcal{B}'_2{}^\dagger = 0, \tag{46}$$

$$M_S^T M_R^{-1} M_S \mathcal{B}'_3{}^\dagger = \mu \mathcal{B}'_1{}^\dagger. \text{ (ignoring less contributing terms)} \tag{47}$$

From the above equations,

$$\mathcal{B}'_1{}^\dagger = M_S^{-1} M_D, \quad \mathcal{B}'_2 = 0, \quad \mathcal{B}'_3{}^\dagger = M_S^{-1} M_R M_S^{T-1} \mu M_S^{-1} M_D. \tag{48}$$

Since  $\mathcal{B}'_2 = 0$ ,

$$\begin{aligned} \mathcal{M}_{\text{light}} = & \left(1 - \frac{1}{2}\mathcal{B}'^{*T}\mathcal{B}'^T\right) (-M_D^T M_R^{-1} M_D) \left(1 - \frac{1}{2}\mathcal{B}'_1 \mathcal{B}'_1^\dagger\right) - \left(1 - \frac{1}{2}\mathcal{B}'^{*T}\mathcal{B}'^T\right) (-M_D^T M_R^{-1} M_S) (\mathcal{B}'_1^\dagger) \\ & - \mathcal{B}'^{*T} (-M_S^T M_R^{-1} M_D) \left(1 - \frac{1}{2}\mathcal{B}'_1 \mathcal{B}'_1^\dagger\right) + \mathcal{B}'^{*T} (\mu - M_S^T M_R^{-1} M_S) \mathcal{B}'_1^\dagger = M_D^T M_S^{-1T} \mu M_S^{-1} M_D, \end{aligned} \quad (49)$$

and,

$$\begin{aligned} \mathcal{M}_{\text{heavy}} = & \mathcal{B}'^{*T} (-M_D^T M_R^{-1} M_D) \mathcal{B}'_1 + \mathcal{B}'^{*T} (-M_D^T M_R^{-1} M_S) \left(1 - \frac{1}{2}\mathcal{B}'_1 \mathcal{B}'_1^\dagger\right) \\ & + \left(1 - \frac{1}{2}\mathcal{B}'^{*T}\mathcal{B}'^T\right) (-M_S^T M_R^{-1} M_D) \mathcal{B}'_1 + \left(1 - \frac{1}{2}\mathcal{B}'^{*T}\mathcal{B}'^T\right) (\mu - M_S^T M_R^{-1} M_S) \left(1 - \frac{1}{2}\mathcal{B}'_1 \mathcal{B}'_1^\dagger\right) \\ = & (\mu - M_S^T M_R^{-1} M_S) + \frac{1}{2} [M_S^T M_R^{-1} M_D M_D^\dagger M_S^{-1\dagger} + \mu M_S^{-1} M_D M_D^\dagger M_S^{-1\dagger} + \text{Trans.}]. \end{aligned} \quad (50)$$

The final block-diagonalized matrix is given by

$$\mathcal{M}_{bd} = \begin{pmatrix} M_D^T M_S^{-1T} \mu M_S^{-1} M_D & 0 & 0 \\ 0 & \mu - M_S^T M_R^{-1} M_S & 0 \\ 0 & 0 & M_R \end{pmatrix}. \quad (51)$$

From Eqs. (42) and (48) we have,

$$\mathcal{U}_1'' = \begin{pmatrix} 1 - \frac{1}{2} M_D^\dagger M_S^{-1\dagger} M_S^{-1} M_D & M_D^\dagger M_S^{-1\dagger} & 0 \\ -M_S^{-1} M_D - M_S^{-1} M_R M_S^{T-1} \mu M_S^{-1} M_D & 1 - \frac{1}{2} M_S^{-1} M_D M_D^\dagger M_S^{-1\dagger} & 0 \\ 0 & 0 & 1 \end{pmatrix}. \quad (52)$$

The final block-diagonalization matrix  $\mathcal{U}_1$  is given by

$$\begin{aligned} \mathcal{U}_1 = & \mathcal{U}_1' \mathcal{U}_1'' \\ = & \begin{pmatrix} 1 - \frac{1}{2} M_D^\dagger M_S^{-1\dagger} M_S^{-1} M_D & M_D^\dagger M_S^{-1\dagger} & M_D^\dagger M_R^{-1} \\ -M_S^{-1} M_D & 1 - \frac{1}{2} M_S^{-1} M_D M_D^\dagger M_S^{-1\dagger} - \frac{1}{2} M_S^\dagger M_R^{-2} M_S & M_S^\dagger M_R^{-1} \\ M_S^{T-1} \mu M_S^{-1} M_D & -M_R^{-1} M_S & 1 - \frac{1}{2} M_R^{-1} M_S M_S^\dagger M_R^{-1} \end{pmatrix}. \end{aligned} \quad (53)$$

Finally to the leading order the active and heavy neutrino mass matrices are given by

$$m_\nu \sim M_D^T M_S^{-1T} \mu M_S^{-1} M_D, \quad (54)$$

$$m_s \sim \mu - M_S^T M_R^{-1} M_S, \quad (55)$$

$$m_n \sim M_R. \quad (56)$$

In the above, if  $\mu$  is greater than  $|M_S^T M_R^{-1} M_S|$  then  $m_s$  will be defined mainly by  $\mu$  and in the opposite case, it will be dominated by  $|M_S^T M_R^{-1} M_S|$ . If  $\mu \sim |M_S^T M_R^{-1} M_S|$  then we have to consider the next order contribution from Eq. (50). The active and sterile matrices will be diagonalized as

$$U^T m_\nu U = \text{diag}(m_{\nu_i}) \quad (57)$$

$$W_s^T m_s W_s = \text{diag}(m_{s_i}) \quad (58)$$

$$W_N^T m_n W_N = \text{diag}(M_{R_i}). \quad (59)$$

So, the mixing matrix for above block diagonalization can be written as

$$\mathcal{U}_2 = \begin{pmatrix} U & 0 & 0 \\ 0 & W_s & 0 \\ 0 & 0 & W_N \end{pmatrix}. \quad (60)$$

Finally the diagonalization matrix of Eq. (31) can be written as,

$$\mathcal{U} = \begin{pmatrix} (1 - \frac{1}{2}M_D^\dagger M_S^{-1\dagger} M_S^{-1} M_D)U & M_D^\dagger M_S^{-1\dagger} W_s & M_D^\dagger M_R^{-1} W_N \\ -M_S^{-1} M_D U & (1 - \frac{1}{2}M_S^{-1} M_D M_D^\dagger M_S^{-1\dagger} - \frac{1}{2}M_S^\dagger M_R^{-2} M_S)W_s & M_S^\dagger M_R^{-1} W_N \\ M_S^{T-1} \mu M_S^{-1} M_D U & -M_R^{-1} M_S W_s & (1 - \frac{1}{2}M_R^{-1} M_S M_S^\dagger M_R^{-1})W_N \end{pmatrix}. \quad (61)$$

## References

- [1] N. Okada, Y. Orikasa, and T. Yamada, *Minimal Flavor Violation in the Minimal  $U(1)_{B-L}$  Model and Resonant Leptogenesis*, Phys. Rev. D **86** (2012) 076003, [[arXiv:1207.1510](#)].
- [2] S. Iso, N. Okada, and Y. Orikasa, *Resonant Leptogenesis in the Minimal B-L Extended Standard Model at TeV*, Phys. Rev. D **83** (2011) 093011, [[arXiv:1011.4769](#)].
- [3] P. Minkowski,  *$\mu \rightarrow e\gamma$  at a Rate of One Out of  $10^9$  Muon Decays?*, Phys. Lett. B **67** (1977) 421–428.
- [4] M. Gell-Mann, P. Ramond, and R. Slansky, *Complex Spinors and Unified Theories*, Conf. Proc. C **790927** (1979) 315–321, [[arXiv:1306.4669](#)].
- [5] T. Yanagida, *Horizontal gauge symmetry and masses of neutrinos*, Conf. Proc. C **7902131** (1979) 95–99.
- [6] R. N. Mohapatra and G. Senjanovic, *Neutrino Mass and Spontaneous Parity Nonconservation*, Phys. Rev. Lett. **44** (1980) 912.
- [7] G. Bambhaniya, P. S. Bhupal Dev, S. Goswami, S. Khan, and W. Rodejohann, *Naturalness, Vacuum Stability and Leptogenesis in the Minimal Seesaw Model*, Phys. Rev. D **95** (2017), no. 9 095016, [[arXiv:1611.03827](#)].
- [8] T. Hambye and D. Teresi, *Higgs doublet decay as the origin of the baryon asymmetry*, Phys. Rev. Lett. **117** (2016), no. 9 091801, [[arXiv:1606.00017](#)].
- [9] P. A. Ade, N. Aghanim, M. Arnaud, M. Ashdown, J. Aumont, C. Baccigalupi, A. Banday, R. Barreiro, J. Bartlett, N. Bartolo, et al., *Planck 2015 results-xiii. cosmological parameters*, Astronomy & Astrophysics **594** (2016) A13.
- [10] M. Fukugita and T. Yanagida, *Baryogenesis Without Grand Unification*, Phys. Lett. **B174** (1986) 45–47.
- [11] M. K. Parida and B. P. Nayak, *Singlet Fermion Assisted Dominant Seesaw with Lepton Flavor and Number Violations and Leptogenesis*, Adv. High Energy Phys. **2017** (2017) 4023493, [[arXiv:1607.07236](#)].
- [12] D. Borah, M. K. Das, and A. Mukherjee, *Common origin of nonzero  $\theta_{13}$  and baryon asymmetry of the Universe in a TeV scale seesaw model with  $A_4$  flavor symmetry*, Phys. Rev. D **97** (2018), no. 11 115009, [[arXiv:1711.02445](#)].
- [13] A. Ibarra, E. Molinaro, and S. T. Petcov, *TeV Scale See-Saw Mechanisms of Neutrino Mass Generation, the Majorana Nature of the Heavy Singlet Neutrinos and  $(\beta\beta)_{0\nu}$ -Decay*, JHEP **09** (2010) 108, [[arXiv:1007.2378](#)].

- [14] A. Granelli, K. Moffat, and S. T. Petcov, *Flavoured Resonant Leptogenesis at Sub-TeV Scales*, [arXiv:2009.03166](#).
- [15] A. Biswas, S. Choubey, L. Covi, and S. Khan, *Common origin of baryon asymmetry, dark matter and neutrino mass*, [JHEP](#) **05** (2019) 193, [[arXiv:1812.06122](#)].
- [16] S. Davidson, E. Nardi, and Y. Nir, *Leptogenesis*, [Phys. Rept.](#) **466** (2008) 105–177, [[arXiv:0802.2962](#)].
- [17] A. Pilaftsis, *The Little Review on Leptogenesis*, [J. Phys. Conf. Ser.](#) **171** (2009) 012017, [[arXiv:0904.1182](#)].
- [18] V. Rubakov and M. Shaposhnikov, *Electroweak baryon number nonconservation in the early universe and in high-energy collisions*, [Usp. Fiz. Nauk](#) **166** (1996) 493–537, [[hep-ph/9603208](#)].
- [19] W. Buchmuller, P. Di Bari, and M. Plumacher, *Some aspects of thermal leptogenesis*, [New J. Phys.](#) **6** (2004) 105, [[hep-ph/0406014](#)].
- [20] M. Plumacher, *Baryogenesis and lepton number violation*, [Z. Phys. C](#) **74** (1997) 549–559, [[hep-ph/9604229](#)].
- [21] G. Giudice, A. Notari, M. Raidal, A. Riotto, and A. Strumia, *Towards a complete theory of thermal leptogenesis in the SM and MSSM*, [Nucl. Phys. B](#) **685** (2004) 89–149, [[hep-ph/0310123](#)].
- [22] A. Pilaftsis and T. E. Underwood, *Resonant leptogenesis*, [Nucl. Phys. B](#) **692** (2004) 303–345, [[hep-ph/0309342](#)].
- [23] T. Hambye, *Leptogenesis at the TeV scale*, [Nucl. Phys. B](#) **633** (2002) 171–192, [[hep-ph/0111089](#)].
- [24] T. Hambye, J. March-Russell, and S. M. West, *TeV scale resonant leptogenesis from supersymmetry breaking*, [JHEP](#) **07** (2004) 070, [[hep-ph/0403183](#)].
- [25] M. Kawasaki, K. Kohri, and T. Moroi, *Big-bang nucleosynthesis and hadronic decay of long-lived massive particles*, [Phys. Rev. D](#) **71** (Apr, 2005) 083502.
- [26] J. Schechter and J. W. F. Valle, *Neutrino masses in  $su(2) \otimes u(1)$  theories*, [Phys. Rev. D](#) **22** (Nov, 1980) 2227–2235.
- [27] **KamLAND-Zen** Collaboration, A. Gando et al., *Search for Majorana Neutrinos near the Inverted Mass Hierarchy Region with KamLAND-Zen*, [Phys. Rev. Lett.](#) **117** (2016), no. 8 082503, [[arXiv:1605.02889](#)]. [Addendum: [Phys.Rev.Lett.](#) **117**, 109903 (2016)].
- [28] S. K. Kang and C. S. Kim, *Extended double seesaw model for neutrino mass spectrum and low scale leptogenesis*, [Phys. Lett. B](#) **646** (2007) 248–252, [[hep-ph/0607072](#)].
- [29] L. Basso, A. Belyaev, S. Moretti, and C. H. Shepherd-Themistocleous, *Phenomenology of the minimal B-L extension of the Standard model: Z' and neutrinos*, [Phys. Rev. D](#) **80** (2009) 055030, [[arXiv:0812.4313](#)].
- [30] P. Galison and A. Manohar, *TWO Z's OR NOT TWO Z's?*, [Phys. Lett. B](#) **136** (1984) 279–283.

- [31] K. S. Babu, C. F. Kolda, and J. March-Russell, *Implications of generalized  $Z - Z'$ -prime mixing*, Phys. Rev. D **57** (1998) 6788–6792, [[hep-ph/9710441](#)].
- [32] A. Leike, *The Phenomenology of extra neutral gauge bosons*, Phys. Rept. **317** (1999) 143–250, [[hep-ph/9805494](#)].
- [33] R. N. Mohapatra and J. W. F. Valle, *Neutrino Mass and Baryon Number Nonconservation in Superstring Models*, Phys. Rev. D **34** (1986) 1642.
- [34] R. N. Mohapatra, *Mechanism for Understanding Small Neutrino Mass in Superstring Theories*, Phys. Rev. Lett. **56** (1986) 561–563.
- [35] D. Wyler and L. Wolfenstein, *Massless Neutrinos in Left-Right Symmetric Models*, Nucl. Phys. B **218** (1983) 205–214.
- [36] E. Witten, *New Issues in Manifolds of  $SU(3)$  Holonomy*, Nucl. Phys. B **268** (1986) 79.
- [37] J. L. Hewett and T. G. Rizzo, *Low-Energy Phenomenology of Superstring Inspired  $E(6)$  Models*, Phys. Rept. **183** (1989) 193.
- [38] A. G. Dias, C. A. de S. Pires, P. S. Rodrigues da Silva, and A. Sampieri, *A Simple Realization of the Inverse Seesaw Mechanism*, Phys. Rev. D **86** (2012) 035007, [[arXiv:1206.2590](#)].
- [39] P. S. B. Dev and R. N. Mohapatra, *TeV Scale Inverse Seesaw in  $SO(10)$  and Leptonic Non-Unitarity Effects*, Phys. Rev. D **81** (2010) 013001, [[arXiv:0910.3924](#)].
- [40] S. Blanchet, P. S. B. Dev, and R. N. Mohapatra, *Leptogenesis with TeV Scale Inverse Seesaw in  $SO(10)$* , Phys. Rev. D **82** (2010) 115025, [[arXiv:1010.1471](#)].
- [41] A. Ilakovac and A. Pilaftsis, *Flavor violating charged lepton decays in seesaw-type models*, Nucl. Phys. B **437** (1995) 491, [[hep-ph/9403398](#)].
- [42] F. Deppisch and J. W. F. Valle, *Enhanced lepton flavor violation in the supersymmetric inverse seesaw model*, Phys. Rev. D **72** (2005) 036001, [[hep-ph/0406040](#)].
- [43] C. Arina, F. Bazzocchi, N. Fornengo, J. C. Romao, and J. W. F. Valle, *Minimal supergravity sneutrino dark matter and inverse seesaw neutrino masses*, Phys. Rev. Lett. **101** (2008) 161802, [[arXiv:0806.3225](#)].
- [44] M. Malinsky, T. Ohlsson, Z.-z. Xing, and H. Zhang, *Non-unitary neutrino mixing and CP violation in the minimal inverse seesaw model*, Phys. Lett. B **679** (2009) 242–248, [[arXiv:0905.2889](#)].
- [45] M. Hirsch, T. Kernreiter, J. C. Romao, and A. Villanova del Moral, *Minimal Supersymmetric Inverse Seesaw: Neutrino masses, lepton flavour violation and LHC phenomenology*, JHEP **01** (2010) 103, [[arXiv:0910.2435](#)].
- [46] J. R. Ellis, D. V. Nanopoulos, and K. A. Olive, *Flipped heavy neutrinos: From the solar neutrino problem to baryogenesis*, Phys. Lett. B **300** (1993) 121–127, [[hep-ph/9211325](#)].
- [47] K. Kannike, *Vacuum Stability Conditions From Copositivity Criteria*, Eur. Phys. J. C **72** (2012) 2093, [[arXiv:1205.3781](#)].
- [48] J. Chakraborty, P. Konar, and T. Mondal, *Copositive Criteria and Boundedness of the Scalar Potential*, Phys. Rev. D **89** (2014), no. 9 095008, [[arXiv:1311.5666](#)].

- [49] **ALEPH, DELPHI, L3, OPAL, LEP Electroweak** Collaboration, S. Schael et al., *Electroweak Measurements in Electron-Positron Collisions at W-Boson-Pair Energies at LEP*, Phys. Rept. **532** (2013) 119–244, [[arXiv:1302.3415](#)].
- [50] M. Carena, A. Daleo, B. A. Dobrescu, and T. M. Tait, *Z' gauge bosons at the Tevatron*, Phys. Rev. D **70** (2004) 093009, [[hep-ph/0408098](#)].
- [51] **ATLAS** Collaboration, M. Aaboud et al., *Search for new high-mass phenomena in the dilepton final state using 36 fb<sup>-1</sup> of proton-proton collision data at  $\sqrt{s} = 13$  TeV with the ATLAS detector*, JHEP **10** (2017) 182, [[arXiv:1707.02424](#)].
- [52] W. Grimus and L. Lavoura, *The Seesaw mechanism at arbitrary order: Disentangling the small scale from the large scale*, JHEP **11** (2000) 042, [[hep-ph/0008179](#)].
- [53] M. Mitra, G. Senjanovic, and F. Vissani, *Neutrinoless Double Beta Decay and Heavy Sterile Neutrinos*, Nucl. Phys. B **856** (2012) 26–73, [[arXiv:1108.0004](#)].
- [54] F. Capozzi, E. Lisi, A. Marrone, and A. Palazzo, *Current unknowns in the three neutrino framework*, Prog. Part. Nucl. Phys. **102** (2018) 48–72, [[arXiv:1804.09678](#)].
- [55] I. Esteban, M. Gonzalez-Garcia, A. Hernandez-Cabezudo, M. Maltoni, and T. Schwetz, *Global analysis of three-flavour neutrino oscillations: synergies and tensions in the determination of  $\theta_{23}$ ,  $\delta_{CP}$ , and the mass ordering*, JHEP **01** (2019) 106, [[arXiv:1811.05487](#)].
- [56] **T2K** Collaboration, K. Abe et al., *Constraint on the matter–antimatter symmetry-violating phase in neutrino oscillations*, Nature **580** (2020), no. 7803 339–344, [[arXiv:1910.03887](#)]. [Erratum: Nature 583, E16 (2020)].
- [57] **NOvA** Collaboration, M. A. Acero et al., *First Measurement of Neutrino Oscillation Parameters using Neutrinos and Antineutrinos by NOvA*, Phys. Rev. Lett. **123** (2019), no. 15 151803, [[arXiv:1906.04907](#)].
- [58] S. Antusch, J. Kersten, M. Lindner, and M. Ratz, *Running neutrino masses, mixings and CP phases: analytical results and phenomenological consequences*, Nuclear Physics B **674** (2003), no. 1 401–433.
- [59] A. Mukherjee, D. Borah, and M. K. Das, *Common Origin of Non-zero  $\theta_{13}$  and Dark Matter in an S<sub>4</sub> Flavour Symmetric Model with Inverse Seesaw*, Phys. Rev. D **96** (2017), no. 1 015014, [[arXiv:1703.06750](#)].
- [60] R. Krishnan, A. Mukherjee, and S. Goswami, *Realization of the minimal extended seesaw mechanism and the TM<sub>2</sub> type neutrino mixing*, JHEP **20** (2020) 050, [[arXiv:2001.07388](#)].
- [61] W. Buchmuller, P. Di Bari, and M. Plumacher, *Leptogenesis for pedestrians*, Annals Phys. **315** (2005) 305–351, [[hep-ph/0401240](#)].
- [62] P. Konar, A. Mukherjee, A. K. Saha, and S. Show, *A dark clue to seesaw and leptogenesis in a pseudo-Dirac singlet doublet scenario with (non)standard cosmology*, [arXiv:2007.15608](#).
- [63] E. Majorana, *Teoria simmetrica dell'elettrone e del positrone*, Nuovo Cim. **14** (1937) 171–184.

- [64] G. Racah, *On the symmetry of particle and antiparticle*, Nuovo Cim. **14** (1937) 322–328.
- [65] W. H. Furry, *On transition probabilities in double beta-disintegration*, Phys. Rev. **56** (1939) 1184–1193.
- [66] W. Rodejohann, *Neutrino-less Double Beta Decay and Particle Physics*, Int. J. Mod. Phys. E **20** (2011) 1833–1930, [[arXiv:1106.1334](#)].
- [67] J. D. Vergados, H. Ejiri, and F. Šimkovic, *Neutrinoless double beta decay and neutrino mass*, Int. J. Mod. Phys. E **25** (2016), no. 11 1630007, [[arXiv:1612.02924](#)].
- [68] S. Dell’Oro, S. Marcocci, M. Viel, and F. Vissani, *Neutrinoless double beta decay: 2015 review*, Adv. High Energy Phys. **2016** (2016) 2162659, [[arXiv:1601.07512](#)].
- [69] S. M. Bilenky and C. Giunti, *Neutrinoless double-beta decay: A brief review*, Mod. Phys. Lett. A **27** (2012) 1230015, [[arXiv:1203.5250](#)].
- [70] A. Meroni, S. T. Petcov, and F. Simkovic, *Multiple CP non-conserving mechanisms of  $(\beta\beta)_{0\nu}$ -decay and nuclei with largely different nuclear matrix elements*, JHEP **02** (2013) 025, [[arXiv:1212.1331](#)].
- [71] J. T. Penedo and S. T. Petcov, *The  $10^{-3}$  eV frontier in neutrinoless double beta decay*, Phys. Lett. B **786** (2018) 410–417, [[arXiv:1806.03203](#)].
- [72] **GERDA** Collaboration, M. Agostini et al., *Improved Limit on Neutrinoless Double- $\beta$  Decay of  $^{76}\text{Ge}$  from GERDA Phase II*, Phys. Rev. Lett. **120** (2018), no. 13 132503, [[arXiv:1803.11100](#)].
- [73] **EXO-200** Collaboration, J. B. Albert et al., *Search for Majorana neutrinos with the first two years of EXO-200 data*, Nature **510** (2014) 229–234, [[arXiv:1402.6956](#)].
- [74] H. V. Klapdor-Kleingrothaus et al., *Latest results from the Heidelberg-Moscow double beta decay experiment*, Eur. Phys. J. A **12** (2001) 147–154, [[hep-ph/0103062](#)].
- [75] **IGEX** Collaboration, C. E. Aalseth et al., *The IGEX Ge-76 neutrinoless double beta decay experiment: Prospects for next generation experiments*, Phys. Rev. D **65** (2002) 092007, [[hep-ex/0202026](#)].
- [76] **NEMO** Collaboration, J. Argyriades et al., *Measurement of the Double Beta Decay Half-life of Nd-150 and Search for Neutrinoless Decay Modes with the NEMO-3 Detector*, Phys. Rev. C **80** (2009) 032501, [[arXiv:0810.0248](#)].
- [77] **CUORE** Collaboration, C. Arnaboldi et al., *CUORE: A Cryogenic underground observatory for rare events*, Nucl. Instrum. Meth. A **518** (2004) 775–798, [[hep-ex/0212053](#)].
- [78] H. V. Klapdor-Kleingrothaus and I. V. Krivosheina, *The evidence for the observation of  $0\nu\beta\beta$  decay: The identification of  $0\nu\beta\beta$  events from the full spectra*, Mod. Phys. Lett. A **21** (2006) 1547–1566.
- [79] **CUORICINO** Collaboration, C. Arnaboldi et al., *Results from a search for the  $0$  neutrino beta beta-decay of Te-130*, Phys. Rev. C **78** (2008) 035502, [[arXiv:0802.3439](#)].
- [80] **NEMO** Collaboration, X. Sarazin and D. Lalanne, *Status report on the double beta decay experiment NEMO-3*, in 30th International Conference on High-Energy Physics, 6, 2000. [hep-ex/0006031](#).

- [81] I. Abt et al., *A New  $Ge^{76}$  Double Beta Decay Experiment at LNGS: Letter of Intent*, [hep-ex/0404039](#).
- [82] H. V. Klapdor-Kleingrothaus, I. V. Krivosheina, A. Dietz, and O. Chkvorets, *Search for neutrinoless double beta decay with enriched  $Ge-76$  in Gran Sasso 1990-2003*, Phys. Lett. B **586** (2004) 198–212, [[hep-ph/0404088](#)].
- [83] **EXO-200** Collaboration, E. Conti et al., *Correlated fluctuations between luminescence and ionization in liquid xenon*, Phys. Rev. B **68** (2003) 054201, [[hep-ex/0303008](#)].
- [84] **Majorana** Collaboration, V. E. Guiseppe et al., *The Majorana Neutrinoless Double-Beta Decay Experiment*, in *2008 IEEE Nuclear Science Symposium and Medical Imaging Conference and 16th International Workshops*, pp. 1793–1798, 2008. [arXiv:0811.2446](#).
- [85] **SuperNEMO** Collaboration, R. Arnold et al., *Probing New Physics Models of Neutrinoless Double Beta Decay with SuperNEMO*, Eur. Phys. J. C **70** (2010) 927–943, [[arXiv:1005.1241](#)].
- [86] J. W. Beeman et al., *Discrimination of alpha and beta/gamma interactions in a  $TeO_2$  bolometer*, Astropart. Phys. **35** (2012) 558–562, [[arXiv:1106.6286](#)].
- [87] **COBRA** Collaboration, T. Bloxham et al., *First results on double beta decay modes of  $Cd$ ,  $Te$  and  $Zn$  isotopes with the COBRA experiment*, Phys. Rev. C **76** (2007) 025501, [[arXiv:0707.2756](#)].
- [88] K. Zuber, *COBRA: Double beta decay searches using CdTe detectors*, Phys. Lett. B **519** (2001) 1–7, [[nucl-ex/0105018](#)].
- [89] **NEXT** Collaboration, F. Granena et al., *NEXT, a HPGXe TPC for neutrinoless double beta decay searches*, [arXiv:0907.4054](#).